SCIEPublish

Review

Recent Advancements in Alumina-Based High-Temperature Insulating Materials: Properties, Applications, and Future Perspectives

Yufei Sun, Suya Li, Qi Zhao, Zihan Cong, Yuguo Xia, Xiuling Jiao and Dairong Chen *

National Engineering Research Center for Colloidal Materials, School of Chemistry and Chemical Engineering, Shandong University, Jinan 250100, China; yfsun622@mail.sdu.edu.cn (Y.S.); syli@mail.sdu.edu.cn (S.L.); zqzhaoqi@mail.sdu.edu.cn (Q.Z.); 202420346@mail.sdu.edu.cn (Z.C.); xyg@sdu.edu.cn (Y.X.); jiaoxl@sdu.edu.cn (X.J.)

* Corresponding author. E-mail: cdr@sdu.edu.cn (D.C.)

Received: 27 November 2024; Accepted: 3 January 2025; Available online: 9 January 2025

ABSTRACT: As a high-temperature thermal insulation material with excellent mechanical properties, alumina (Al_2O_3)-based materials hold significant potential for applications in aerospace, advanced manufacturing, automobiles, industrial furnaces, and other fields. However, the inherent brittleness of alumina poses a limitation to its wider application. Therefore, there is a pressing need to develop alumina-based materials that offer high toughness while retaining superior mechanical properties. This paper begins by exploring the structure of alumina, highlighting its thermal conductivity, insulation, and mechanical properties in high-temperature environments. It then reviews the classification and synthesis methods of alumina-based materials, along with the latest advances in design strategies. Notably, the rational design of alumina composition, structure, and morphology is emphasized as crucial for optimizing material performance, thereby supporting the industrial development and application of these materials in high-tech sectors. Finally, the paper discusses the challenges and evolution of alumina-based materials in real-world industrial applications and suggests potential directions for future development.

Keywords: Alumina-based materials; High-temperature; Insulating materials; Synthesis; Aerospace applications; Industrial furnace applications; Environmentally friendly materials

1. Introduction

High-temperature technology is important in many industries, such as primary metal and non-metal production, materials processing, chemicals, transportation, and power generation [1]. Among these, insulation materials are critical for thermal management and protection systems [2–4]. Thermal insulation has been used for many years as one of the key components in installations and industrial facilities, especially in pipelines, tanks, and heat exchangers, but it is also used in the building industry, power engineering, the chemical process industry, refrigeration, firemanship, and aeronautics.

High-temperature insulation materials (or combinations of materials) are designed to limit the transfer of heat between an insulated object and its surrounding environment. These materials are primarily classified based on their internal structure into three categories: (1) fibrous materials, such as mineral wool and glass wool; (2) cellular materials, such as foam glass and polyurethane foam; and (3) granular materials, including powders and diatomaceous earth. Insulation materials are complex, multi-component substances with heterogeneous properties. They generally exist in three aggregate states: (1) solid, composed of particles, fibers, and matrix (e.g., foamed insulation); (2) liquid, where the insulation contains water; and (3) gaseous, such as air, water vapor, or other gases. The selection of insulation type and thickness depends on various factors, including thermal performance and technical and economic considerations influenced by physical properties such as low thermal conductivity (high thermal resistance), low apparent density, and high compressive strength. Today, the focus is on expanding the applications of insulation materials, improving existing solutions, and developing new materials that can more effectively reduce heat transfer.

https://doi.org/10.70322/htm.2025.10001

Alumina-based materials are used in a wide range of applications in advanced manufacturing, aerospace, automotive, industrial furnaces, and other areas. This is due to the high mechanical strength, corrosion resistance, and excellent thermal stability of these materials. Alumina is very important in the production of ceramic materials and can be used to make products that are more resistant to wear, including grinding media, abrasives, and cutting tools. In addition, alumina ceramics are used for components in harsh environments, including gas turbines and automotive components, due to their high melting point (over 2000 °C) and resistance to thermal shock. Alumina ceramics have a lower thermal conductivity than metals, good thermal stability, and high mechanical strength. They are commonly used in the field of high-temperature insulation and are a major strategic material for national development [5]. Alumina-based insulation materials mainly include aerogel [6], powders [7], and coated forms [8] of structure. In short, alumina-based materials are indispensable materials for modern industry.

Nevertheless, alumina-based materials continue to encounter numerous obstacles in actual industrial applications and production processes, which constrains the rate of their advancement and utilization. Ideal alumina-based materials should possess the following characteristics: (1) While ensuring excellent mechanical properties, they should also exhibit sufficient toughness to prevent cracking when subjected to external impact, which would otherwise result in catastrophic damage to the mechanical properties [9]. (2) The production conditions should be mild, the energy consumption should be low, the process parameters should be easily controllable, and the production cost should be low when scaled up [10,11]. (3) The production process should be environmentally friendly, free from pollution, with minimal waste and optimal resource utilization [12]. It is, therefore, crucial to elucidate the intricate interrelationships between composition, structure, process, and performance, and to devise innovative preparation processes and recycling technologies with a view to promoting the utilization of alumina-based materials in industrial and high-tech applications [13,14].

The objective of this paper is to introduce alumina-based high-temperature insulating materials. The paper begins by examining the relationship between the structure and properties of alumina. It then turns to the characteristics that are conducive to the development of high-tech fields. Furthermore, it reviews the latest progress in the classification, synthesis methods, and design strategies of alumina-based materials. It also explores the current development direction of Al_2O_3-based materials. In particular, it emphasizes that the rational design of alumina composition, structure, and morphology is conducive to regulating the performance of materials. This, in turn, facilitates the industrialization of alumina-based materials. In conclusion, the paper considers the prospective developments and challenges of alumina-based materials in practical industrial applications, offering insights to facilitate pivotal breakthroughs in high-tech and industrial large-scale production.

2. Fundamentals of Alumina-Based Materials

2.1. The Structure of Alumina

Aluminium is the third most prevalent element in the Earth's crust, accounting for 7.45% of the total crustal weight. Aluminum compounds are plentiful, with the most prevalent being aluminum oxide (Al_2O_3), aluminum oxide monohydrate (AlOOH), and aluminum oxide trihydrate or hydroxide ($Al(OH)_3$). These compounds also exhibit a number of distinct subtypes, as illustrated in Table 1 [15]. Alumina exhibits a high degree of polymorphism, displaying over ten distinct crystal forms, including α-, β-, γ-, δ-, θ-, η-, χ-, and others. The structures and properties of the various crystal forms exhibit notable differences. The arrangement structure of O^{2-} can be classified into two main types: face-centered cubic (FCC) and hexagonal closest packed arrangement (HCP). Subsequent division into different phases is dependent on the distinct sublattices of Al^{3+}. The synthesis of alumina crystals with varying properties can be achieved through the manipulation of the raw materials and the preparation process. The most prevalent alumina crystalline forms and their associated transformation temperatures are presented in Figure 1 [16].

Table 1. Common Al_2O_3 crystal forms.

Types	Crystal Forms	JCPDS No.	Density (g/cm^3)
γ-Al_2O_3	Cubie spinel	00-010-0425	3.67
δ-Al_2O_3	Tetragonal	00-046-1131	3.65
θ-Al_2O_3	Monoclinic	00-011-0517	3.59
η-Al_2O_3	Cubic	01-077-0396	-
χ-Al_2O_3	-	00-004-0880	-
κ-Al_2O_3	Orthorhombic	01-088-0107	3.75
α-Al_2O_3	Rhombohedral	00-042-1468	3.98

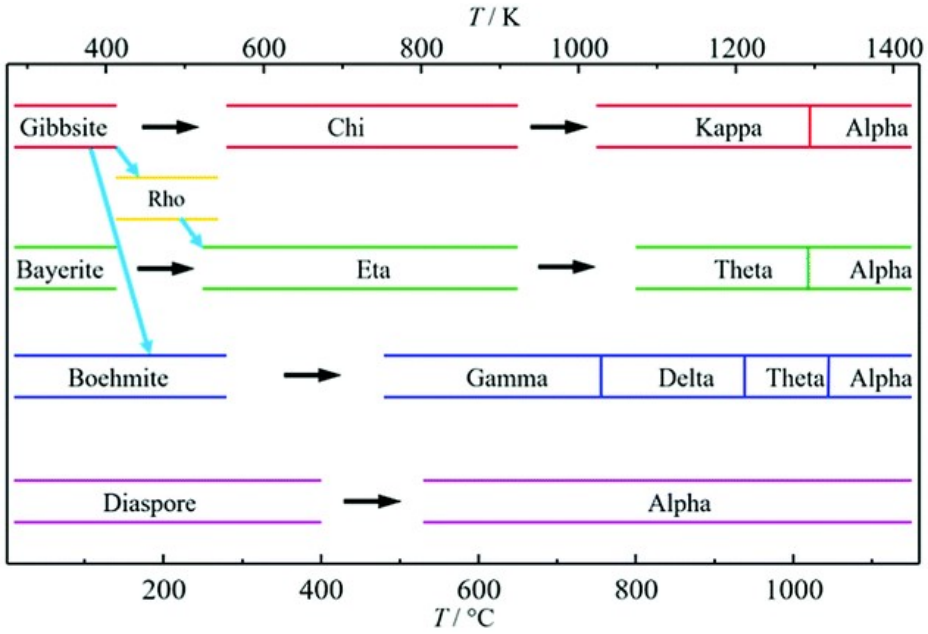

Figure 1. Schematic representation of the thermal evolution of transition alumina phases in air. Schematic representation of the thermal evolution (black arrows) of transition alumina phases in air, from the hydroxide and oxyhydroxide precursors, gibbsite, boehmite, bayerite and diaspore.The non-thermal transformations are shown with blue arrows.

The most common and widely used crystal forms of alumina are γ-Al_2O_3 and α-Al_2O_3. γ-Al_2O_3, also designated as activated alumina, is classified as a transitional alumina. It has a cubic crystal structure, analogous to that of the $MgAl_2O_4$ lattice, and displays a defective spinel structure [17]. In this structure, the oxygen ions occupy the eight vertices of the cubic lattice, thereby forming a cubic close-packed crystal framework. The aluminum ions are randomly distributed within the gaps of the crystal structure, which is composed of oxygen ions in the form of octahedral or tetrahedral coordination. However, due to the discrepancy in the ratio of anions to cations, the gaps are not filled, with hydroxyl groups occupying some of the vacancies left by aluminum ions. The removal of hydroxyl groups at elevated temperatures will result in alterations to the crystal structure, ultimately leading to the formation of denser α-Al_2O_3, accompanied by a reduction in volume and the release of heat. The γ-Al_2O_3 crystal structure is characterized by a loose arrangement of particles, which exhibit a porous, small-spherical morphology. It exhibits the characteristics of a large specific surface area, high activity, and strong adsorption capacity. It can be employed as an adsorbent, dehydrating agent, catalyst, and carrier. γ-Al_2O_3 is not a naturally occurring substance; it can only be produced through the process of artificial synthesis [18].

α-Al_2O_3 is the most stable alumina crystal phase [19]. The most common forms found in nature are natural corundum and sapphire. The space group is $R\bar{3}C$, and the lattice constants are a = 0.475 nm and c = 1.297 nm, with a *Z*-value of 6. The oxygen ions within the α-Al_2O_3 crystal structure are arranged in a hexagonal close-packed structure, forming a crystal skeleton in which the ions are stacked in the order A-B-A-B. The remaining aluminum ions are situated within the octahedral voids of the lattice. To maintain electrical neutrality, the aluminum ions occupy only two-thirds of the octahedral voids. This configuration results in a highly compact crystal structure of α-Al_2O_3, while simultaneously ensuring the electrical neutrality of the ions within. This ordered structure provides the basis for the excellent performance of α-Al_2O_3, making it highly applicable in a range of fields, including ceramics, abrasives, grinding tools, and refractory materials [20].

2.2. Thermal Conductivity and Insulation Properties

The thermal insulation properties of alumina (Al_2O_3) are mainly reflected in its low thermal conductivity, which is a key parameter in measuring the material's thermal insulation properties. The thermal conductivity of alumina is dependent upon the crystal structure, density, and purity of the material. Typically, the value can reach to 30 $W \cdot m^{-1} \cdot K^{-1}$ [21]. The process of heat conduction in alumina is determined by the vibration of the lattice, which is referred to as phonons. The oxygen atoms are closely arranged with the aluminum atoms to form a highly ordered crystal structure, and the thermal conductivity changes with different grain sizes [22]. The phonon thermal conductivity (κph) follows the law $\kappa \sim T^{-1}$ at room temperature. As the temperature increases, the phonon scattering rate increases, resulting in a decrease in κph. Therefore, the thermal conductivity of alumina shows a decreasing trend with increasing temperature.

Figure 2 shows the thermal conductivity of alumina as a function of temperature. Nevertheless, alumina materials exhibit lower thermal conductivity and superior high-temperature stability in comparison to metal materials. Consequently, they are frequently employed in the fabrication of high-temperature thermal insulation materials [23]. The thermal insulation properties of alumina are mainly related to its porous and low-density structure. This structure requires heat transfer to occur through the gas in the pores in addition to solid phase conduction, greatly extending the heat transfer path and effectively blocking heat transfer. Liu et al. [24] prepared amorphous hollow alumina with an average diameter of 181 nm and a shell thickness of less than 10 nm. The application of hollow alumina for thermal insulation, combined with ordinary fiberglass insulation, reduced the thermal conductivity by 30% to 0.028 $W \cdot m^{-1} \cdot K^{-1}$ compared to pure fiberglass, while maintaining good fire resistance and elasticity. The thermal conductivity of the composite (42 wt% alumina) remains virtually unchanged at temperatures ranging from 100 to 400 °C, providing good high-temperature stability.

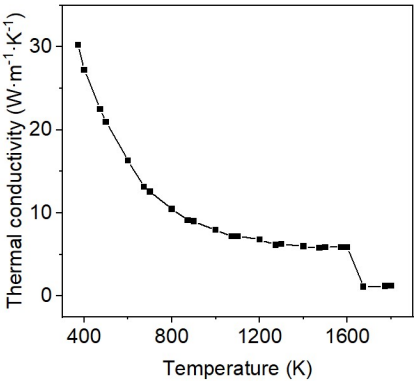

Figure 2. Thermal conductivity of aluminum oxide as a function of temperature.

2.3. Mechanical Properties at High Temperatures

Alumina materials exhibit a range of exceptional properties, including high strength, high hardness, wear resistance, favorable chemical stability, and heat resistance. At elevated temperatures, the mechanical properties of alumina exhibit intricate alterations, influenced by a multitude of variables. The flexural and compressive strengths of 99.5% alumina ceramics are 2350 MPa and 350 MPa, respectively [25]. However, as the temperature rises, its strength declines gradually. A notable decline in strength is observed when the temperature exceeds 1200 °C. At elevated temperatures, the crystal structure of aluminum oxide changes, resulting in an uneven distribution of stress within the material and a concomitant reduction in strength. On the other hand, an increase in temperature will result in the expansion of cracks within the material, which will have a significant impact on the mechanical properties [26]. Moreover, the relatively stable nature of the covalent bonds of alumina at high temperatures means that the hardness of alumina is not significantly reduced. Creep is defined as the permanent deformation of a material over time under constant stress. It is an important indicator of long-term stability. As the temperature rises, the migration of atoms or ions between the lattice of alumina-based materials becomes more facile, leading to creep and subsequent plastic deformation. Consequently, the plasticity and toughness of the material are enhanced to a certain extent at elevated temperatures [27]. However, it remains challenging to meet the requirements of industrial applications. The thermal expansion coefficient of alumina materials is closely related to the crystal form. α-Al_2O_3 is relatively stable and has a low thermal expansion coefficient, while γ-Al_2O_3 has a higher thermal expansion coefficient and may undergo phase changes at high temperatures, thereby affecting the dimensional stability of the material.

2.4. Types of Alumina-Based Materials

2.4.1. Monolithic Alumina Ceramics

Alumina ceramics, also referred to as corundum ceramics, are a category of ceramic material comprising primarily of aluminum oxide (Al_2O_3) (Figure 3a–c) [28]. They possess a range of advantageous properties, including high-temperature resistance, corrosion resistance, wear resistance, and high hardness. The aluminum oxide content is a determining factor in the performance and utilization of alumina ceramics [29]. Consequently, alumina ceramics can be categorized according to the aluminum oxide content, with high-purity alumina ceramics (99.9% Al_2O_3) and ordinary alumina ceramics representing the two main divisions. The industry further subdivides ordinary alumina ceramics into

the following categories: “99 porcelain” (99% Al_2O_3), “95 porcelain” (95% Al_2O_3), “90 porcelain” (90% Al_2O_3), “85 porcelain” (85% Al_2O_3), and “75 porcelain” (75% Al_2O_3). A material is no longer classified as an alumina ceramic if its alumina content is less than 75%.

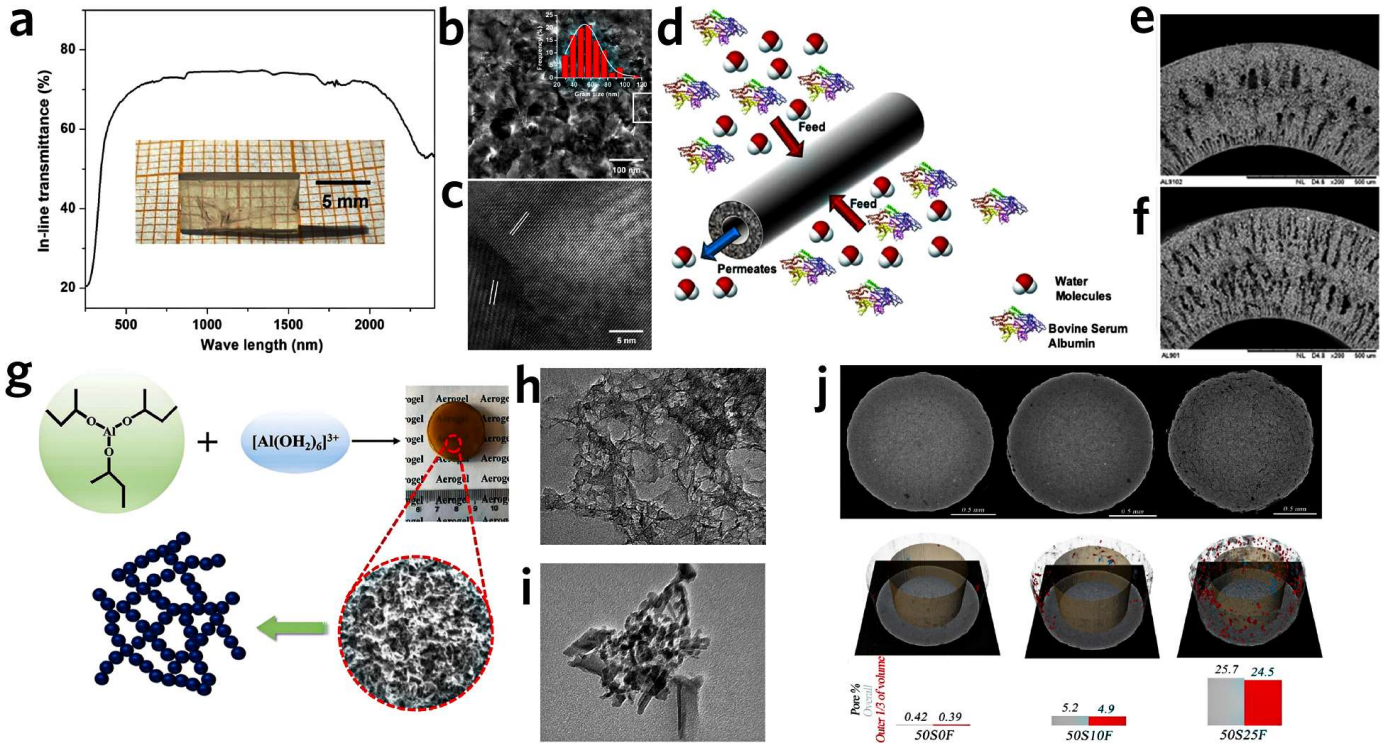

Figure 3. (**a**) Optical transmission spectra of transparent alumina synthesized under 5.0 GPa/600 °C. Inset image is a rectangular crack-free slice cutting out along the axial direction of the sample. (**b**) TEM image of the sample (inset image shows the grain size distribution of the sample). (**c**) Curvilinear grain boundary between two nanograins. (**d**) Schematic diagram of an alumina hollow fiber membrane in which finger-like structures were formed both on the inside of the lumen and on the outside of the membrane surface, while sponge-like were formed in the middle of the membrane. High-resolution TEM image of the area indicated by white rectangle in (**e**,**f**), showing the transformed super fine grains among larger grains. (**g**–**i**) Aluminum oxide aerogel and TEM image. (**j**) Micro-CT images of zirconia-reinforced alumina ceramic matrix composites.

2.4.2. Alumina Fibers and Aerogels

Alumina fiber is a high-performance, polycrystalline inorganic fiber comprising Al_2O_3 as the principal component (Figure 3d–f) [30]. The material displays excellent high-temperature oxidation resistance, is lightweight, exhibits corrosion resistance, has low thermal conductivity, demonstrates good thermal stability, and offers a high cost-performance ratio. To satisfy the diverse functional requirements, the form of the material is typically classified into three categories: whiskers, short fibers, and continuous fibers. Amorphous alumina typically exhibits a series of phase transitions under high-temperature firing conditions, accompanied by the formation of various metastable alumina crystal forms, including γ, δ, and θ. Ultimately, it transforms to α-Al_2O_3, which exhibits relatively stable thermodynamic properties. However, α-Al_2O_3 is susceptible to fracture due to its high degree of crystallinity. At elevated temperatures for extended periods, the grains of this material increase in size, leading to a reduction in strength. Accordingly, a modest quantity of SiO_2 is typically incorporated during the preparation process to impede the growth of its grains and reinforce the crystal phase [31].

Alumina aerogel is a highly porous and low-density material composed of nanoparticles of aluminum oxide. The complex three-dimensional network structure and nano-scale pores of alumina aerogel significantly inhibit solid-state and gaseous heat conduction, resulting in an extremely low thermal conductivity (Figure 3g–i) [32]. Due to the high proportion of gas within its volume, the material exhibits low density and excellent thermal insulation. Furthermore, it exhibits the high-temperature resistance and chemical stability characteristic of Al_2O_3, retaining its nanoporous structure even at 1000 °C.

2.4.3. Alumina-Based Composites

The ongoing advancement of science and technology has led to a notable surge in demand for high-performance materials. The inherent performance limitations of traditional single materials have rendered them unsuitable for modern applications, thus giving rise to the development of composite materials. Alumina-based composites are composite materials formed by combining an Al_2O_3 matrix with other reinforcements (Figure 3j) [33]. Such composites are typically employed to enhance mechanical properties and address the brittleness and poor toughness of alumina. The morphology of the reinforcement phase allows for the classification of these composites into three main categories: fiber reinforcement (such as whiskers and short fibers), particle reinforcement, and other types. Among these, whisker reinforcement (e.g., SiC_w, Mu_f), particle reinforcement (e.g., Cu, Ti, Al_2O_3, SiC, ZrO_2), and short fiber reinforcement (e.g., Al_2O_{3f}, C_f, SiC_f) are classified as discontinuous phase reinforcement. The reinforcement mechanism of the reinforcement phase can be broadly categorized into three main areas: phase transformation toughening, crack deflection, and elastic modulus mismatch between particles and the matrix. In comparison to discontinuous phase reinforcement, continuous phase fibers (such as SiO_2, ZrO_2, MgO_2) can be dispersed more evenly when combined with the alumina matrix. This avoids the catastrophic damage to the material that would otherwise result from brittle fracture caused by stress concentration [34–36].

3. Synthesis and Production Methods

There are many methods to prepare alumina-based high-temperature insulating materials. The traditional methods mainly include sol-gel, roll forming, *etc.*, of which sol-gel is the most commonly used method. In addition, with the rise of new technologies, the preparation of alumina-based high-temperature insulation materials by 3D printing and other methods also has a good development prospect.

3.1. Sol-Gel Method

Most alumina aerogels are synthesized by the sol-gel method, which mainly relies on the hydrolysis of precursors such as alkoxides or inorganic salts to produce reactive monomers, which undergo a series of polymerization, solubilization, and gelation to produce precursors, and finally undergo different drying methods to obtain the final aerogel structure. Zhang et al. prepared Al_2O_3/SiC composite aerogel, as shown in Figure 4a, and evaluated its thermal insulation performance through the ablation of a butane blowtorch (above 1000 °C) [37]. Figure 4b shows the infrared image of composite aerogel exposed to a butane burner flame for 120 s. During the whole heating process, the back surface temperature of composite aerogel was kept below 200 °C. It was further found in the experiment (Figure 4c) that the higher the content of SiC nanowires, the slower the rise rate of their back surface temperature. This is because the SiC nanowires were oxidized into SiO_2. When the heating temperature rose, the protective layer would delay the further erosion of the composite aerogel framework structure. F. Peng et al. developed a direct sol-immersion-gel (SIG) and supercritical fluid drying (SCFD) strategy (as shown in Figure 4d) for the synthesis of mullite fiber reinforced alumina-silica aerogel composites (MFAS) [38]. As shown in Figure 4e–h, they studied the relationship function between the thermal conductivity dilution of MFAS and fiber density, temperature, and air pressure. Figure 4i shows the heat transfer mechanism of MFAS. With the cooperation of alumina-silica aerogel (ASA) and mullite fiber, MFAS shows a quite low thermal conductivity (down to 0.082 $W \cdot m^{-1} \cdot K^{-1}$ even at 1200 °C), indicating that mullite fiber greatly inhibits radiation heat transfer. At the same time, MFAS is compared with other alumina-based aerogel composites. As shown in Figure 4j, MFAS has excellent thermal insulation performance, the thermal conductivity at 1200 °C is 25% lower than the best value ever mentioned.

Zu et al. have developed an acetone-aniline in situ water formation (AISWF) sol-gel technique (Figure 5a), which can effectively slow down the hydrolysis and condensation rate of the highly reactive metal alkoxide by controlling water formation through slow dehydration reaction of acetone and aniline [39]. The core-shell Al_2O_3 aerogel/mullite fiber/TiO_2 composite possesses ultralow thermal conductivities of 0.058, 0.080, and 0.11 $W \cdot m^{-1} \cdot K^{-1}$ at 800, 1000, and 1200 °C, respectively, which are the lowest values for inorganic aerogels ever reported (Figure 5b). The core-shell Al_2O_3 aerogel shows much lower thermal conductivity compared to that of the pristine one after heat treatment at high temperatures (Figure 5c). Figure 5d shows the comparison between the thermal conductivity of core-shell Al_2O_3 aerogel and other related materials reported in the literature. It can be seen that the core-shell Al_2O_3 aerogel gel has more excellent thermal insulation performance under high-temperature conditions. Huang et al. proposed a novel fiber-reinforced and opacified (FRO) strategy to fabricate the ZrO_2 fiber-reinforced alumina-silica aerogel composites (ZFASA) (Figure 5e) that boast ultra-low thermal conductivity (0.031 $W \cdot m^{-1} \cdot K^{-1}$ at 1100 °C) [40]. ZFASA exhibits

remarkable thermal stability, enduring quartz lamp and butane torch tests at 1300 °C without any obvious change (Figure 5f). Ji et al. prepared alumina aerogels with superior ultrahigh-temperature-resistant and thermal insulation were successfully prepared by assembling the α-Al_2O_3 nanosheets with silica sols as the high-temperature binders [41]. Benefiting from the generation of the mullite-covered alumina biphasic structure, the α-Al_2O_3 nanosheet-based aerogels (ANSAs) exhibit excellent thermal and chemical stabilities even after calcination at as high as 1600 °C. SiBCN/Al_2O_3 composite aerogel synthesized by Jiang et al. has superior high-temperature structural stability and low thermal conductivity (0.039 $W \cdot m^{-1} \cdot K^{-1}$) [42].

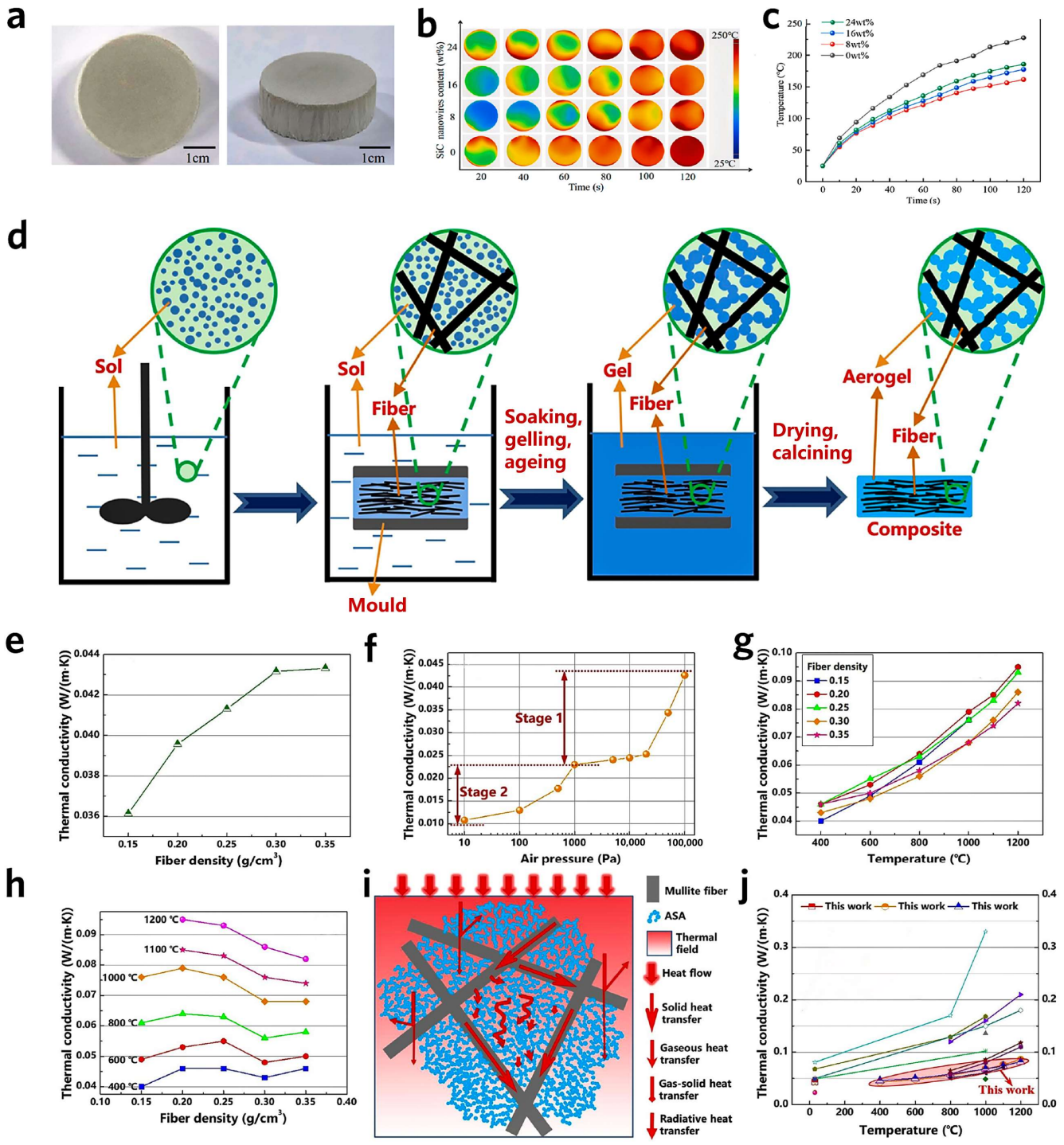

Figure 4. (**a**) Al_2O_3/SiC composite aerogel. (**b**) Infrared image of composite aerogels exposed to a butane blowtorch flame for 120 s. (**c**) Time-dependent temperature evolution of the back face. (**d**) Fabrication of the MFASs through the SIG-SCFD strategy. Thermal insulating properties of the MFASs: Thermal conductivity (air atmosphere, RT) of (**e**) the MFASs as a function of fiber density and of (**f**) the MFAS30 as a function of air pressure; High-temperature thermal conductivities of the composites: as a function of the (**g**) temperature and (**h**) fiber density. (**i**) Heat transfer mechanism in the MFAS. (**j**) Thermal conductivity of the MFASs in this work and alumina-based aerogel composites in previous works.

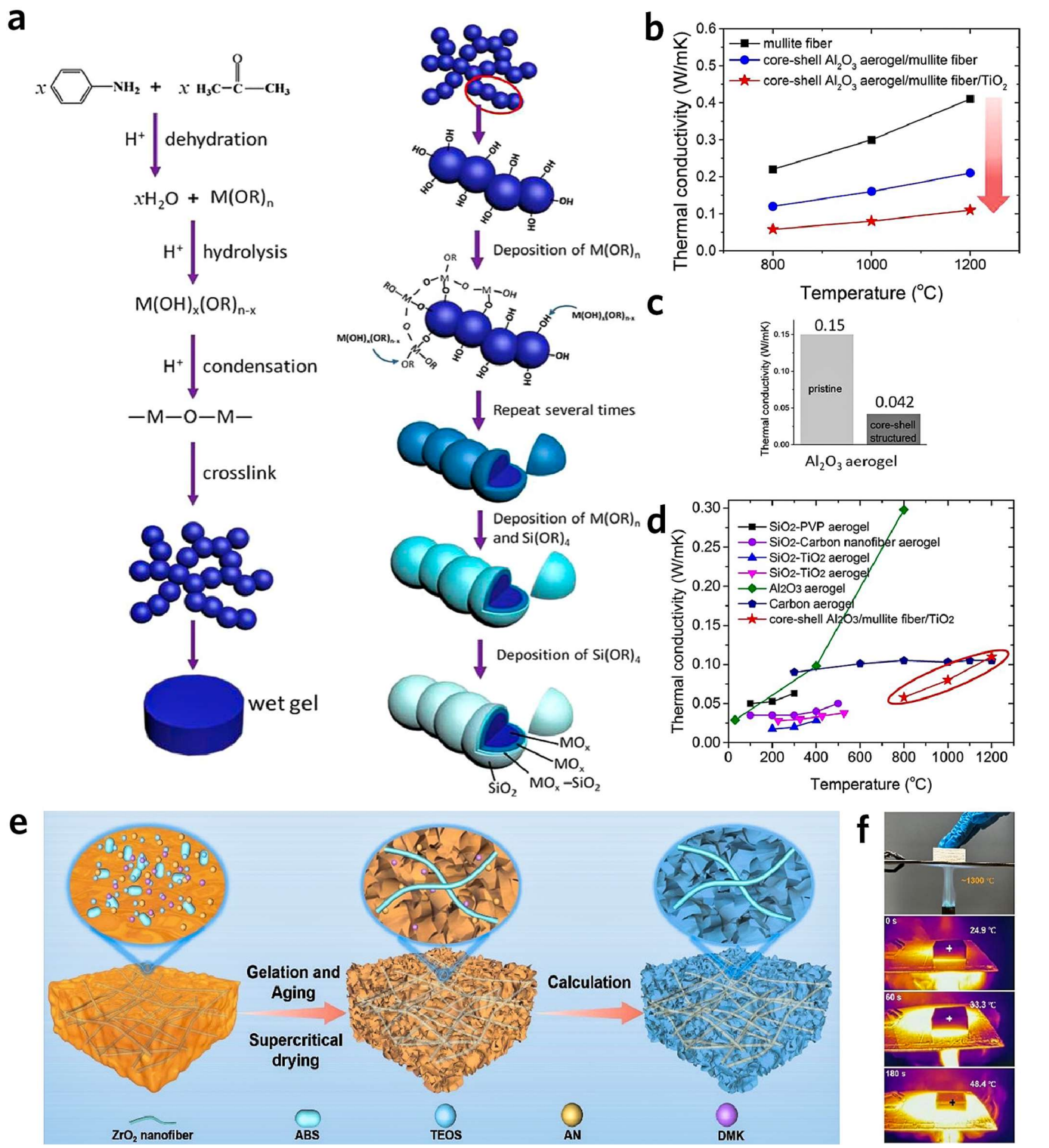

Figure 5. (**a**) AISWF sol−gel process. (**b**) The high-temperature thermal conductivities for the commercial polycrystalline mullite fiber, core−shell Al_2O_3 aerogel/mullite fiber composite, and core−shell Al_2O_3 aerogel/mullite fiber/TiO_2 composite. (**c**) The room-temperature thermal conductivities for the pristine and core−shell nanostructured Al_2O_3 aerogels after heat treatment at 1300 °C. (**d**) Comparison of the high-temperature thermal conductivity values of our core−shell Al_2O_3 aerogel/mullite fiber/TiO_2 composite and the reported aerogels. (**e**) Schematic illustration of the preparation process of ZFASA. (**f**) Schematic illustration of the preparation process of ZFASA and Optical and infrared images of ZFASA under a butane torch.

3.2. Roll Forming

Roll forming refers to the preparation of alumina-based high-temperature insulating materials through rolling extrusion, which has the advantages of low cost, high yield, and easy particle size control. Luo et al. obtained alumina ball blocks of different particle sizes using roll roll-forming method (Figure 6a) [43]. As shown in Figure 6c, the thermal conductivities of these three materials were very close at the same temperature, and as the temperature increased, all

materials had nearly linear growth thermal conductivities. Mixing alumina balls of different particle sizes in a 1:1 mass ratio, Figure 6d showed that the thermal conductivity of multi-particle materials was slightly higher than that of single-particle materials. Liu et al. used ball milling to grind a mixture of nano-Al_2O_3, nano-SiO_2, SiC, and glass fiber and pressed them into a steel mold to prepare a new type of nano alumina silica insulation board with ultra-low thermal conductivity [44]. The preparation process is shown in Figure 6b. As for insulation materials, pore size has a significant impact on thermal conductivity, as shown in Figure 6e. At the same temperature, small pore materials can effectively limit the convective heat transfer of gas molecules due to their pore size being smaller than the average free path of air, thereby achieving lower thermal conductivity. At a certain porosity, the thermal conductivity increases with the increase of testing temperature, which is due to the enhancement of thermal radiation.

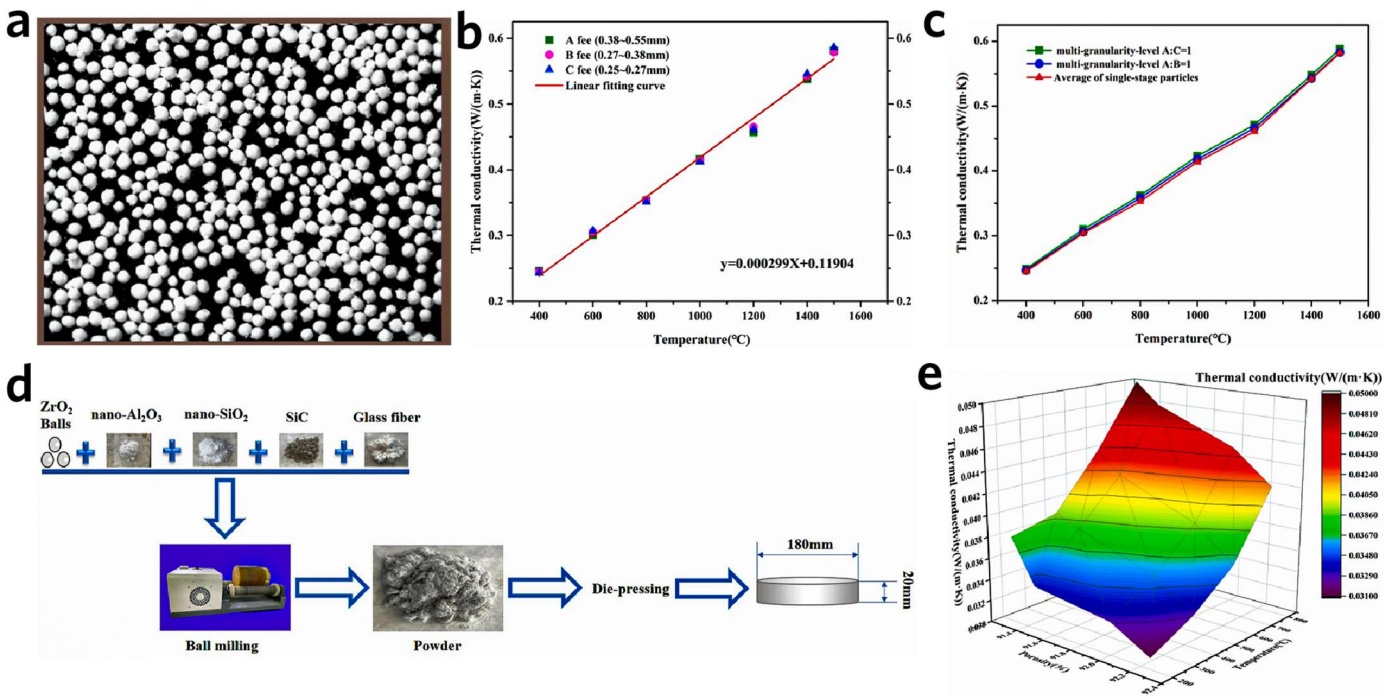

Figure 6. (**a**) macroscopic morphologies of alumina ball bulk material. (**b**)Illustration of the preparation process of novel nanometer alumina-silica insulation board. (**c**) Change of thermal conductivity of multi-granularity-level materials with temperature. (**d**) Change of thermal conductivity of single-granularity-level materials with temperature. (**e**) Thermal conductivity values of novel nanometer alumina-silica insulation board with various porosity and testing.

3.3. 3D Print

The emergence of additive manufacturing (3D printing) technology provides a diverse platform for customized 3D structures and new opportunities for the development of alumina-based insulating materials. Meanwhile, 3D printing can be a good solution to the problem of brittleness in conventional molding and post-processing processes due to the inefficient necking of oxide ceramic nanoparticles. Two structures of alumina (Al_2O_3) ceramics (hollow lattice structure and solid lattice structure) were prepared using DLP 3D printing by Sun et al. [45]. After sintering at 1600 °C for 4 h, dense alumina ceramics with an average grain size of 4.38 ± 1.26 μm were obtained with good molding accuracy and shape. The upper surface temperature of the hollow lattice is 500 °C, and the temperature transferred to the lower surface is only 88.6 °C, which can effectively reduce heat loss and improve energy efficiency. Wang et al. invented a versatile thermal-solidifying direct-ink-writing method with good compatibility and designability for printing alumina-silica aerogels (Figure 7a) [46]. Figure 7b means that ≈70% of the temperature increase has been insulated by the 3D-printed ceramic aerogels and the aerogels had a low thermal conductivity (30.87 $mW \cdot m^{-1} \cdot K^{-1}$) (Figure 7c,d). Yang et al. developed a new three-dimensional printing gel for the construction of hierarchical porous ceramics with tunable millimeter-, micrometer-, and nanometer-sized pores (Figure 7e), and the localized temperature of the chip exposed to the contact heat was only 34.2 °C in the presence of a printed foam cap with a pore size of 41.5 μm, which is 20.6 °C lower than the localized temperature of the pure chip (Figure 7f) [47].

Additionally, the 3D-printed alumina-based ceramic substrates can effectively enhance the stability of capacitors at high temperatures and maintain strong adhesion [48,49]. Obeidat et al. [50] utilized 3D printing technology with alumina to create a matrix for the embedding of radio frequency (RF) chips and the printing of RF transmission lines.

Under thermal cycling (from −55 °C to 125 °C, 100 cycles) and aging (85 °C, 85% relative humidity) conditions, the printed components and RF die units demonstrated good mechanical and electrical properties, as well as robustness and reliability.

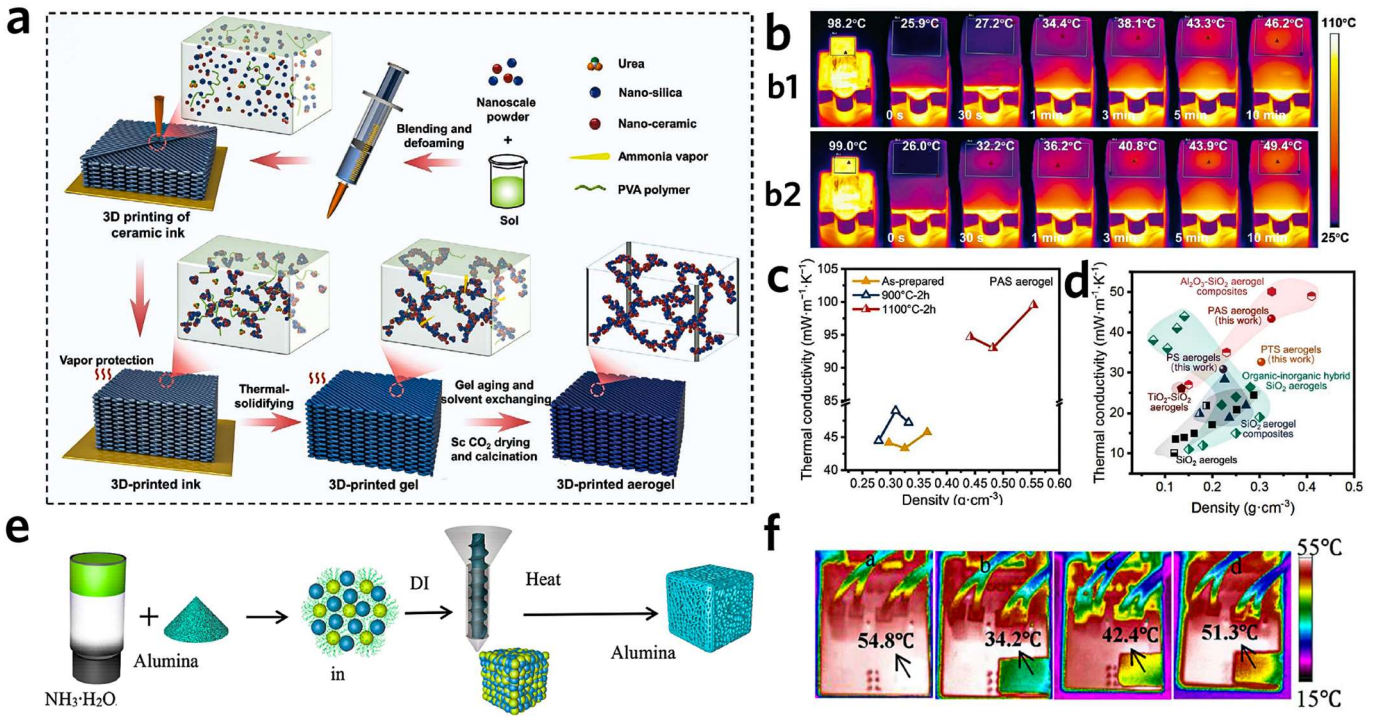

Figure 7. (**a**) Schematic illustration of a versatile thermal-solidifying direct-write assembly to fabricate ceramic aerogels. (**b**) Infrared images of the PTS aerogel shield (**b1**) and PAS aerogel shield (**b2**) installed on the surface of a 100 °C heating source. (**c**) Thermal conductivity versus density for 3D-printed aerogels with different heat treatment temperatures. (**d**) Thermal conductivity versus density for different aerogel materials. (**e**) Schematic Diagram of DIW 3D Printing of Porous Alumina Ceramics. (**f**) Infrared thermal imaging of (a) circuit board without an insulator cap and a circuit board containing an insulator cap made from ceramic foam with pore sizes of (b) 41.5, (c) 83.4, and (d) 137.4 μm.

3.4. Other Methods

In addition to the commonly used methods mentioned above, other scholars have attempted to prepare alumina-based high-temperature insulating materials through various methods. Xia et al. prepared ceramic microspheres from the solid-liquid mixture containing alumina by spray drying and then used to successfully prepare porous mullite ceramics with enhanced compressive strength via a simple direct stacking and sintering approach (Figure 8a) [51]. And calcined them to synthesize porous mullite ceramics, as shown in Figure 8b. Figure 8c shows the effect of sintering time on the thermal diffusion coefficient, specific heat capacity, and thermal conductivity of the prepared porous mullite ceramics. With the passage of time, the thermal diffusion coefficient and thermal conductivity of the sample slowly increased and then sharply increased while the specific heat capacity decreased. This indicated that the thermal insulation performance of the obtained porous ceramics decreased with the extension of sintering time, which was attributed to the decrease in the sample's porosity with the increase of sintering time. On the basis of the gel-sol method, Wang et al. prepared flexible alumina fiber for ultra-fine heat insulation by electrospinning, and its preparation diagram is shown in Figure 8d [52]. As shown in Figure 8e, they studied the thermal conductivity of alumina fibers at different temperatures, and the thermal conductivity gradually increased with increasing temperature. Figure 8f shows the comparison of thermal conductivity between alumina fiber and other materials. Compared with other materials, the alumina fiber prepared in this study at 1000 °C has certain advantages in thermal insulation. Chen et al. constructed a hexagonal boron nitride (h-BN)-Al_2O_3 dual-layer coating structure with an outer alumina coating that effectively shields the space solar thermal (Figure 8g) [8]. In the vertical direction (D⊥), the dual-layer h-BN/Al_2O_3 coating exhibits effective thermal insulation with a considerable reduction in the equilibrium temperature measured at the rear surface (Figure 8h,i).

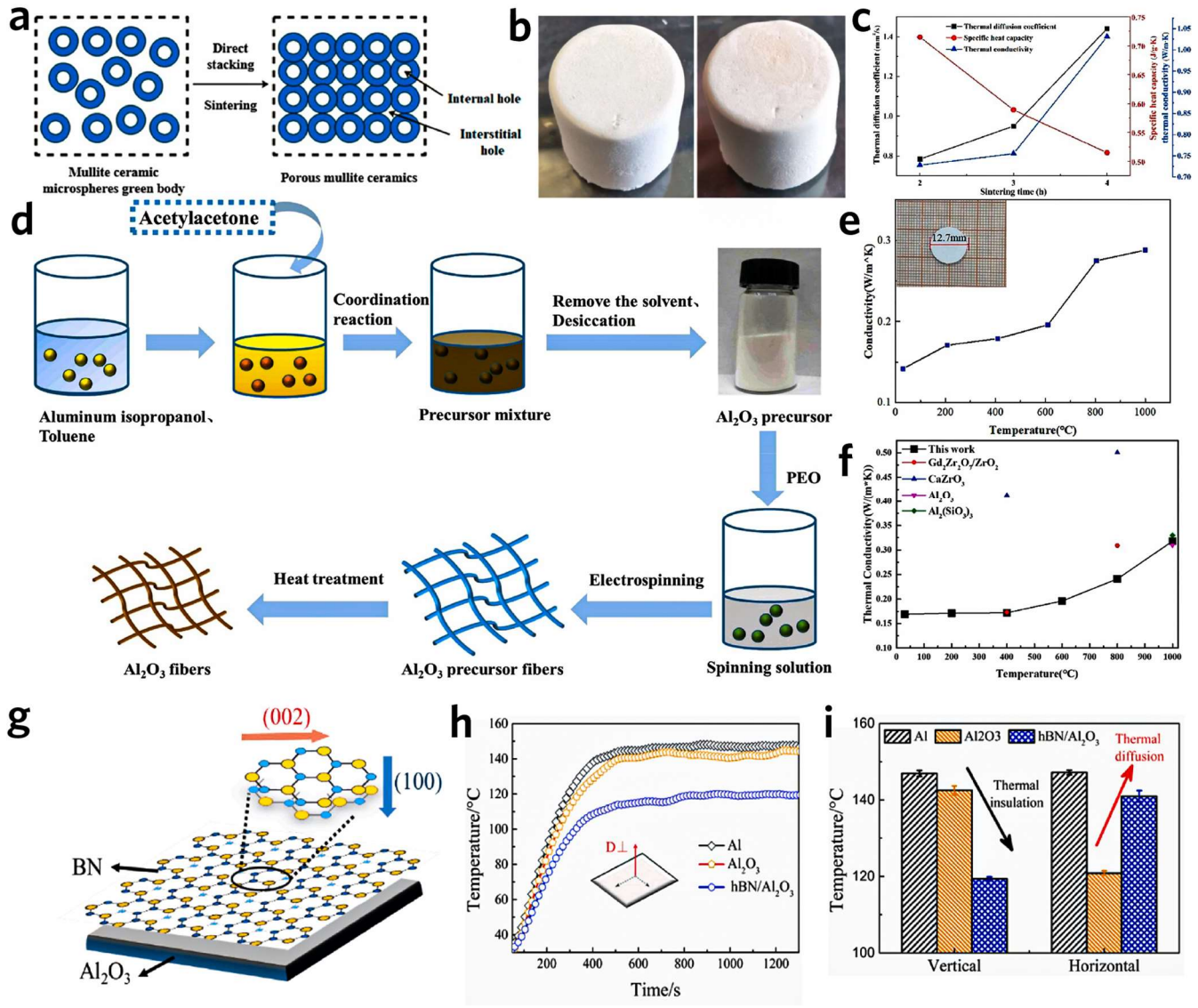

Figure 8. (**a**) Schematic diagram of the synthesis of the lightweight and high-strength mullite ceramics with ceramic microspheres green body by a direct stacking and sintering process. (**b**) Macroscopic digital photos of samples prepared at 1550 °C at different times. (**c**) Variation curves of sample thermal insulation properties with sintering time. (**d**) Schematic view of the production route for alumina fibers. (**e**) Thermal conductivity of Al_2O_3 fibers. (**f**) Comparison figure of thermal conductivity of different materials. (**g**) Schematic of the hBN/Al_2O_3 dual-layers coating, designed for space radiative cooling. Comparison of temperature evolutions for Al substrate, Al_2O_3, and h-BN/Al_2O_3 coatings in (**h**) vertical (out-of-plane). (**i**) Comparison of the equilibrium temperatures of Al substrate, Al_2O_3, and h-BN/Al_2O_3 coatings in the vertical and horizontal directions.

4. Performance and Applications

Al_2O_3, a widely utilized ceramic material, is renowned for its exceptional hardness, excellent wear resistance, high-temperature stability, and superior electrical insulating properties. These characteristics have made it indispensable across various industries. Notably, the demand for Al_2O_3-based materials is growing in advanced sectors such as aerospace, electronics, energy, metallurgy, and chemical engineering. This chapter aims to explore the directions of research on Al_2O_3-based materials, focusing on the key properties that drive their performance and application in these high-tech fields.

4.1. High-Temperature Stability

Al_2O_3-based materials are extensively employed in high-tech fields due to their exceptional thermal stability and high-temperature resistance. With a melting point of approximately 2050 °C and excellent thermal conductivity, Al_2O_3 maintains remarkable physical stability even in extreme heat environments. Additionally, its low coefficient of thermal expansion allows it to be used over a wide range of temperatures and reduces thermal stresses, minimizing deformation

or cracking of the material due to temperature changes. Al_2O_3 also demonstrates outstanding oxidation and corrosion resistance, maintaining its integrity in the presence of oxygen, moisture, and various acidic and alkaline media.

The high-temperature performance of Al_2O_3-based materials is closely related to their microstructure. Key microstructural factors, such as crystal structure [53] (Figure 9a), grain size [54] (Figure 9b), and phase composition [55] (Figure 9c), have a direct impact on the material's mechanical properties and thermal stability at elevated temperatures. While Al_2O_3-based materials generally exhibit good high-temperature stability, phase transitions and grain growth at elevated temperatures can lead to a degradation of their mechanical properties. Compared to γ-Al_2O_3, α-Al_2O_3 possesses a more stable crystal structure, maintaining its physical and chemical stability at high temperatures, which makes it particularly suitable for high-temperature applications. Furthermore, microstructural defects, such as pores or cracks, can act as sites for stress concentration, thereby reducing the material's compressive strength and service life. Therefore, by optimizing the microstructure, such as controlling the grain size and reducing the porosity, the comprehensive performance of Al_2O_3-based materials can be effectively enhanced in high-temperature environments.

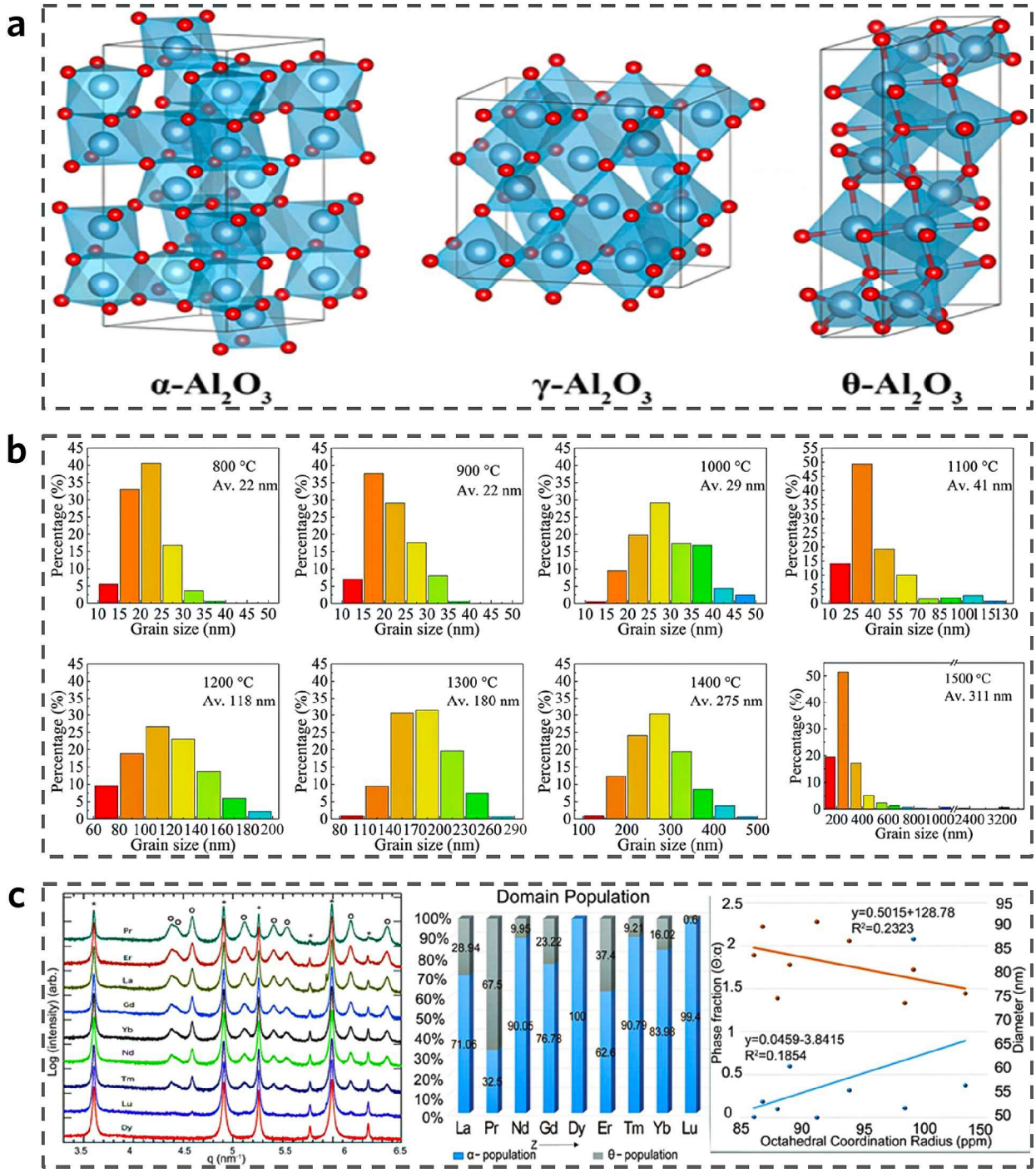

Figure 9. (**a**) Schematic crystal structure of Al_2O_3. (**b**) Temperature on the grain size of Al_2O_3. (**c**) Effect of rare earth metal doping on the composition of crystalline phases.

Lamouri et al. investigated the effect of heating rate on α-Al_2O_3 and found that α-Al_2O_3 exhibits a denser and more homogeneous microstructure with fewer pores, higher density, and well-defined grain boundaries at a heating rate of 5 °C·min^{-1} (Figure 10a) [56]. The observed pore densification was attributed to the formation of a rough, worm-like pore structure during the phase transition of Al_2O_3. Liu et al. employed ZIF-8 as a carbon source to in situ create carbon nanonetworks derived from MOFs at the grain boundaries of zirconia-toughened alumina (ZTA) ceramics through discharge plasma sintering (Figure 10c) [57]. At a MOF concentration of 1.0–2.0 wt%, the ZTA ceramics demonstrated the highest bending strength (719 ± 20.5 MPa) and fracture toughness (7.91 ± 0.7 MPa·m$^{1/2}$), which were 1.37 and 1.88 times greater, respectively, than those of the unmodified samples. The MOF-derived carbon nanonetworks effectively dispersed internal stresses and redirected concentrated stresses from defects to the two-phase grain boundaries, enhancing both the reinforcement and toughening properties of the material.

Furthermore, the thermal stability of Al_2O_3-based composites can be further optimized through the doping of various elements or the incorporation of other ceramic materials. The thermal stability of Al_2O_3-based materials can be enhanced by incorporating small amounts of sintering additives. Commonly used sintering additives include rare earth metals and transition metal oxides or non-oxides. The addition of these materials can modify the crystal structure of Al_2O_3, thereby improving phase stability. To prevent segregation and agglomeration, the content of these additives is typically kept below 5 wt%. Doping with rare earth metal ions can effectively inhibit grain growth during sintering, suppress the high-temperature phase transitions of Al_2O_3, and significantly improve the thermal stability of the material. Transition metals, on the other hand, can prevent further oxidation of Al_2O_3 by forming a stable oxide film, particularly at elevated temperatures and in high oxygen environments. This doping strategy enhances the antioxidant properties of the material. Overall, these doping techniques can substantially extend the service life of Al_2O_3-based materials, especially in extreme high-temperature conditions, while significantly boosting their overall performance. MgO can be incorporated into Al_2O_3 fibers to investigate the evolution of their microstructure and its impact on material properties (Figure 10b) [58]. Doping with 2 wt% MgO had been found to inhibit the growth of α-Al_2O_3 crystals and accelerate grain refinement. The grain growth index increased by 3.2 during prolonged holding at 1100 °C, suggesting that MgO-doped Al_2O_3 fibers exhibit improved thermal stability. Jiang et al. prepared N610f/SiO_2 composites via a sol-gel process, sintered at temperatures ranging from 800 to 1200 °C (Figure 10d) [59]. At the critical sintering temperature of 1200 °C, the SiO_2 matrix underwent a phase transition, leading to a significant increase in Young's modulus and hardness. Due to weak fiber/matrix interfacial interactions, N610f/SiO_2 composites sintered at 800 and 1000 °C exhibited quasi-ductile fracture behavior. Higher sintering temperatures resulted in a stronger SiO_2 matrix and enhanced interfacial strength, which contributed to the brittle fracture behavior of the composites. Dong et al. prepared Al_2O_3-ZrO_2 nanofibers via electrospinning, followed by the fabrication of nanofiber-based porous ceramics through gelation, freeze-drying, and high-temperature sintering [60]. The introduction of ZrO_2 inhibited grain growth at elevated temperatures, and after sintering at 1400 °C, the resulting ceramics exhibited a multilayered pore structure with high thermal stability, ultra-high porosity (97.79–98.04%), ultra-low density (0.075–0.091 g·cm^{-3}), and low thermal conductivity (0.0474–0.0554 W·m^{-1}·K^{-1}). Defective graphene (DG) and Si_3N_4 nw were grown in situ with Al_2O_3 and SiO_2 as the porous skeleton and sintered to construct a homogeneous Si_3N_4nw synergistic DG-reinforced network (Figure 10e) [61]. The optimal flexural strength and fracture toughness of the sintered ceramics were 388.52 MPa and 11.29 MPa·m$^{1/2}$, respectively, due to the refinement of ceramic grains by DG and the consumption of additional energy by Si_3N_4nw during the plucking process.

The thermal stability of Al_2O_3-based materials is influenced by a range of factors, including their crystal structure, impurity composition, and the external environment. By leveraging advanced material design and composite technologies, the thermal stability of these materials can be substantially enhanced, thereby ensuring reliable performance in high-temperature applications.

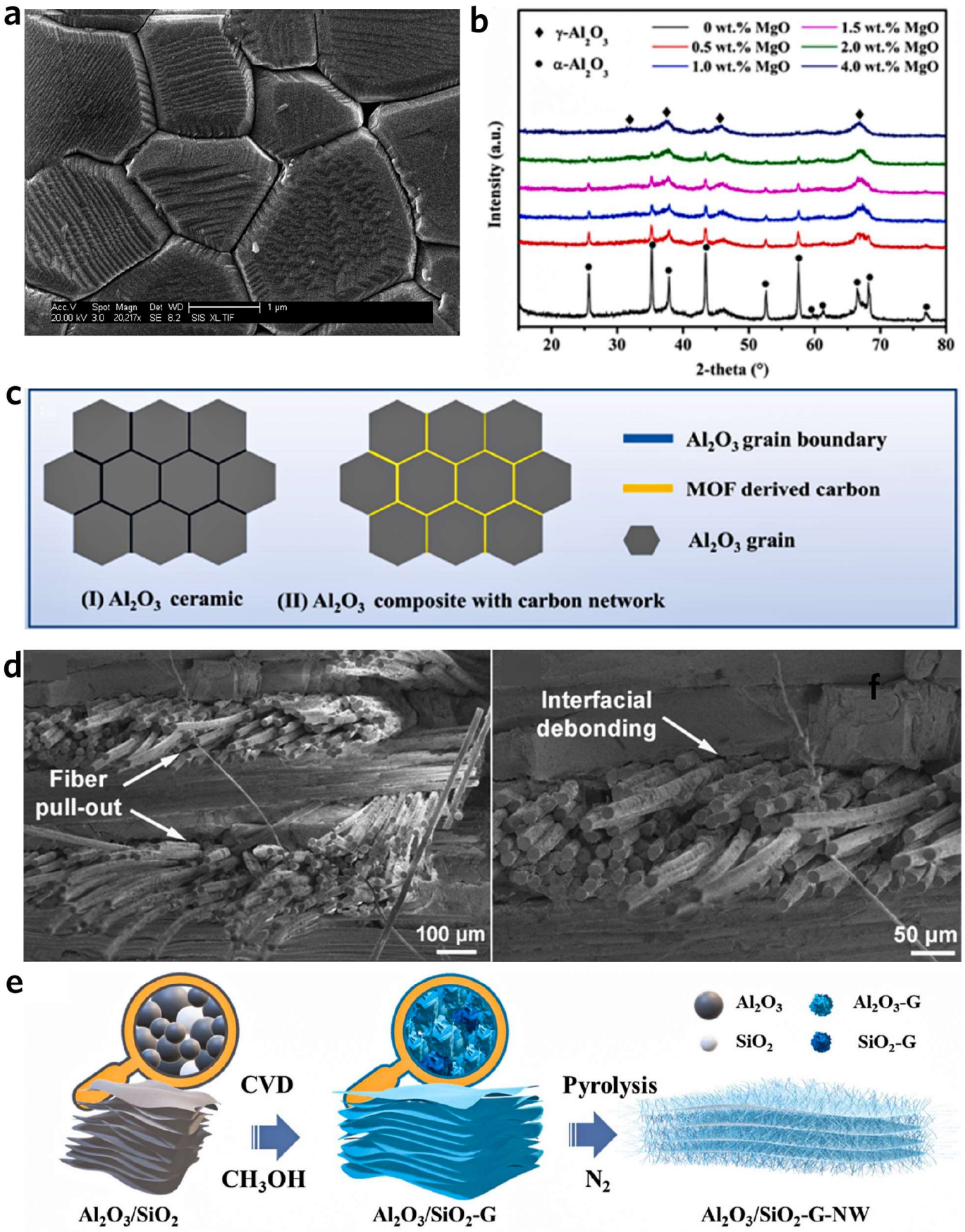

Figure 10. (**a**) SEM showing grains boundaries of γ-Al_2O_3. (**b**) XRD patterns of the sintered alumina fibers with different MgO amounts at 900 °C for 30 min. (**c**) Schematic diagram of designed grain boundary Al_2O_3 and Al_2O_3 composite with continuous ultrafine MOF-derived carbon network structure. (**d**) Fracture morphologies of the N610f/SiO_2 composites fabricated at 800 °C after the three-point-bending tests. (**e**) Preparation process of Al_2O_3/ SiO_2-G-NW.

4.2. Thermal Insulation Efficiency

As the precision of electronic devices increases, the heat dissipation of the components is also facing a great challenge, so the requirements for ceramic substrates are becoming higher and higher. Compared with other ceramics, Al_2O_3-based ceramics have high thermal conductivity, but their excellent cost performance has made them active in the field of thermally conductive ceramics for a long time. How to maximize its advantages is a key topic of current research. Researchers have focused on optimizing the thermal insulation performance of Al_2O_3-based materials through modification and composite design strategies.

To reduce the overall thermal conductivity of Al_2O_3-based materials, it can be combined with other low-thermal-conductivity substances. For instance, the incorporation of aerogel into Al_2O_3 composites significantly enhances their thermal insulation performance due to the aerogel's ultra-low density and extremely low thermal conductivity. In addition, the microstructure of Al_2O_3-based materials plays an important role in determining their thermal insulation properties. Factors such as particle size, porosity, and particle morphology can be optimized to further improve the thermal insulation properties of these materials. He et al. developed mullite fiber insulating tiles coated with $MoSi_2$-borosilicate (MFIT@$MoSi_2$), which demonstrated excellent thermal protection [62]. Even at a heat flux of 450 $kW \cdot m^{-2}$, the surface temperature reached 1043.1 °C, while the cold surface remained close to room temperature. The high emissivity of $MoSi_2$ significantly boosted the radiative heat dissipation from the surface, thereby suppressing both surface and internal temperatures (Figure 11a,b). Furthermore, the bond strength between the coating and substrate remained robust even under challenging conditions involving heating and vibration. Shimizu et al. investigated the thermal conductivity of high-porosity Al_2O_3 foams, which exhibited a density of 0.1 $g \cdot cm^{-3}$ at room temperature and a thermal conductivity of 0.12 $W \cdot m^{-1} \cdot K^{-1}$ [63]. Thermal radiation was found to influence the foam's thermal conductivity at 510 °C, with the conductivity increasing as the temperature rose, whereas the thermal conductivity of Al_2O_3 itself decreased with increasing temperature. Liu et al. combined hollow alumina nanoshells with glass fibers using the high-temperature reduced-jet flame method to produce hollow alumina-glass fiber composites with a thermal conductivity of 0.028 $W \cdot m^{-1} \cdot K^{-1}$, which was 30% lower than that of pure glass fibers (Figure 11c–e) [64].

The thermal insulation performance of Al_2O_3-based materials is influenced not only by their intrinsic properties but also by the processing methods employed during fabrication. For instance, variations in sintering techniques and the inclusion of different sintering additives can alter the density, porosity, and microstructure of Al_2O_3-based materials, thereby impacting their thermal insulation efficiency. In recent years, the application of 3D printing has enabled precise control over the material's structural properties, enhancing both thermal insulation efficiency and mechanical performance. Hossain et al. utilized 3D printing technology to fabricate mullite ceramics from α-Al_2O_3 and SiO_2, which, after high-temperature calcination at 1400 °C, were fully transformed into mullite while maintaining 75% porosity, a cold compressive strength of 8 MPa, and a thermal conductivity of 0.173 $W \cdot m^{-1} \cdot K^{-1}$ (Figure 11f) [65]. Cao et al. employed a 3D printing approach to fabricate porous ceramics using photosensitive hydroxysiloxanes (HPMS-KH570) as the resin matrix [66]. These ceramics exhibited high porosity (79.42%), low density (0.47 $g \cdot cm^{-3}$), and low thermal conductivity (0.11 $W \cdot m^{-1} \cdot K^{-1}$) at room temperature.

There is a correlation between the corrosion resistance and insulation properties of Al_2O_3-based materials. As a chemically stable material, alumina has excellent corrosion resistance to most acids and bases, which allows it to maintain its performance in harsh environmental conditions and can be used to create insulation for use in chemically active or corrosive environments, such as in chemical, petroleum, and aerospace industries. These properties of alumina are particularly important in applications where both corrosion resistance and thermal insulation properties need to be considered, such as high-temperature furnace linings, chemical pipeline insulation, and thermal protection systems for aerospace vehicles. Bie et al. [67] investigated the use of Al_2O_3-SiC-C (ASC) refractory bricks as a chromium-free refractory for applications in gasification furnaces. In the energy industry, the gasification process involves the reaction of fossil fuels with oxygen and water to produce syngas, which are typically operated at 1300–1500 °C and 2.5–6.5 MPa.The ASC material showed better corrosion resistance than the conventional Cr_2O_3-Al_2O_3-ZrO_2 material in tests on coke beds and in air, and can be used as a promising chromium-free gasifier lining material.

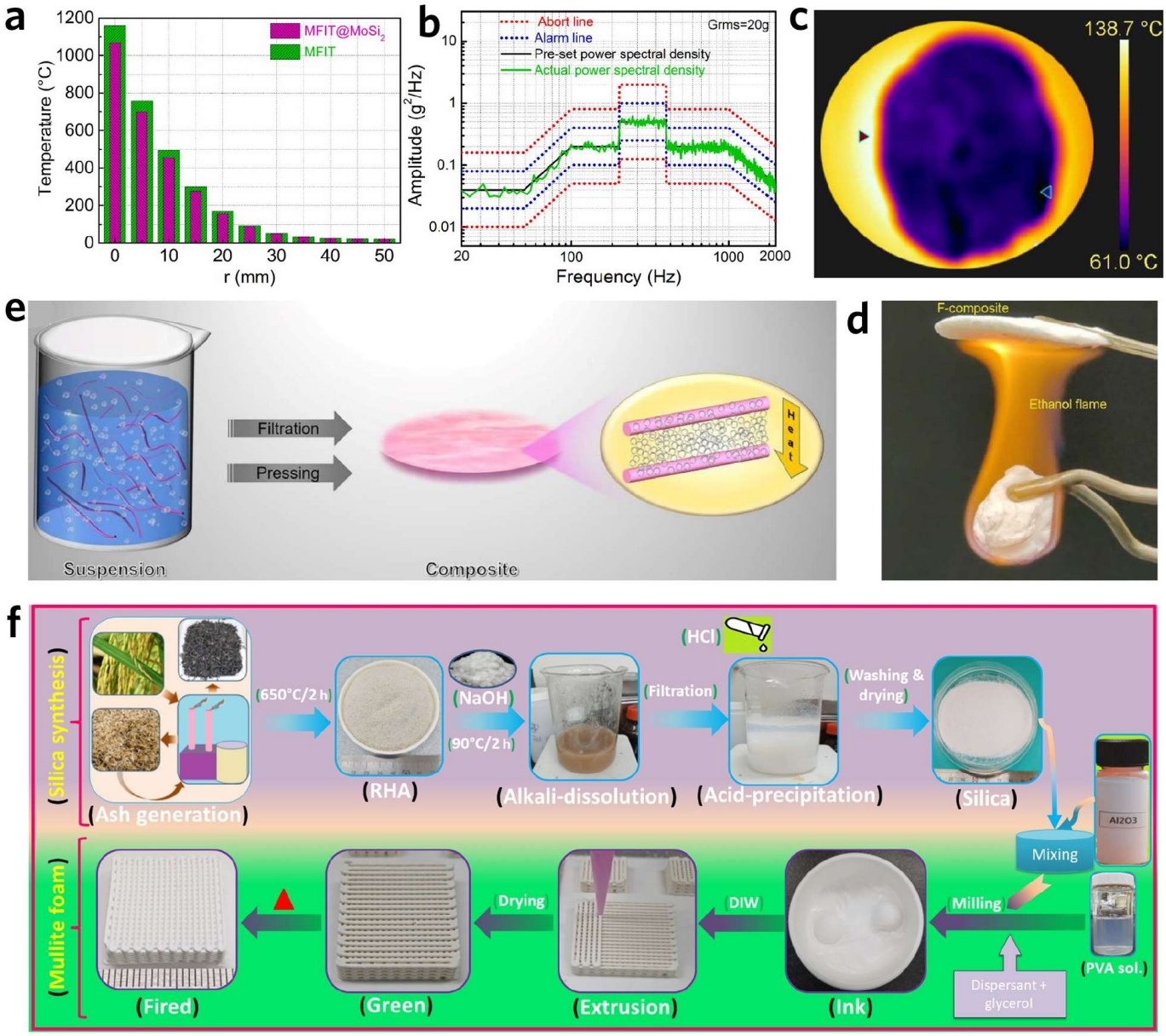

Figure 11. (**a**) Comparative results of the maximum temperatures of MFIT and MFIT@$MoSi_2$ at different positions. (**b**) Power spectral density control curve at Grms = 20 g. (**c**) Infrared image of F-composites on a 140 °C hot plate after 10 min. (**d**) Illustration of the fire resistance of F-composites in an ethanol flame. (**e**) Formation and thermal insulation mechanism of F-composite. (**f**) Scheme for preparing RHA-derived silica and mullite foams.

The potential of Al_2O_3-based insulation materials for applications in high-temperature environments continues to expand with the advancement of new composite materials and processing technologies. Therefore, Al_2O_3-based materials remain a key class of high-performance insulation materials. Future research should focus on the development of multifunctional composites and innovative manufacturing techniques to further improve their overall performance.

4.3. Real-World Applications

Al_2O_3-based materials have excellent high-temperature stability, corrosion resistance, mechanical strength, and low density. They are widely used in industrial and scientific research fields in refractories, abrasives, ceramic products, and other fields due to their excellent properties.

4.3.1. Aerospace and Automotive Industries

Environmental/thermal barrier coatings protect ceramic composites from heat and vapor, prolonging their service life and reducing maintenance costs, thus improving their efficiency and cost-effectiveness. Al_2O_3 relies primarily on its excellent thermal stability, corrosion resistance and high melting point, which gives it excellent protective properties in high-temperature harsh environments. In addition, Al_2O_3 coatings resist oxidation at high temperatures, preventing the formation of oxidized layers on metallic materials at high temperatures. This property is particularly important for applications in high-temperature environments, such as rocket motors and automotive exhaust systems, where effective oxidation protection is required to ensure that equipment performance remains stable under extreme conditions.

With the improvement of science and technology levels, aviation engine technology has made great progress, and the requirements for the power level of the vehicle are getting higher and higher while improving the performance of the aircraft. The most effective way to improve engine performance is by increasing the turbine inlet gas temperature. Due to its lightweight, high strength, and high-temperature resistance, Al_2O_3 ceramics can improve the performance and reliability of aerospace devices, mainly used in engine nozzles and small engine high-temperature parts. Al_2O_3 ceramics have become an ideal material for the manufacture of aircraft engine parts, thermal protection and other key components. For example, the exhaust components of aero-engines, composed of Al_2O_3/Al_2O_3 composite center cones and nozzles, represent the largest Al_2O_3-based components in aero-engines and have successfully completed in-flight testing to TRL7. Xie et al. formed a dense and uniform Al_2O_3 film by thermal atomic layer deposition, which prevented surface oxidation of Al during storage, avoided wastage of material and energy during production, and suppressed secondary electron emission (Figure 12a,b) [68]. Li et al. prepared an Al_2O_3 based ceramic coating with enhanced corrosion resistance and anti-icing properties [69]. The electrochemical corrosion potential of the coating is 70 mV higher than that of the substrate, indicating that the coating has strong corrosion resistance (Figure 12c,d).

In the automotive industry, Al_2O_3-based materials are extensively employed in high-performance systems, including engine components, braking systems, and drivetrains. Their excellent wear resistance enables them to effectively withstand high loads and speeds, thereby improving system reliability and safety. Specifically, Al_2O_3-based materials are used in sealing rings, brake pads, bearings, and other critical components, owing to their resistance to high temperatures, corrosion, and low friction coefficient, which are crucial for the performance of high-performance engines and braking systems. Sousa et al. conducted dry turning experiments using MgO-doped Al_2O_3 ceramic tools on 450-grade peristaltic graphite cast iron to analyze wear mechanisms and surface roughness (Figure 12e,f) [70]. Due to the prolonged contact between the chip and the tool surface, combined with the material's corrosive nature, abrasive wear was found to increase with cutting speed. As a result, abrasion emerged as the predominant wear mechanism across all experimental conditions. In a separate study, Hussainova et al. evaluated the wear behavior of graphene-encapsulated Al_2O_3 composites over several hours [71]. Under mild operating conditions, the wear resistance of these composites was improved by a factor of three compared to pure Al_2O_3, which was used as the reference material. Vanvirsinh et al. treated Al_2O_3 particles with siloxane to improve the adhesion between the filler and the matrix and the wear of the material [72]. The wear resistance of the siloxane-treated gasket is increased by 35%. Shen et al. took 5–200 μm Al_2O_3 nanoparticles as the abrasive to study the wear of the abrasive during reciprocating sliding at room temperature [73]. The evolution trend of abrasive particles with different particle sizes is different. In the process of friction, the amount of wear and friction coefficient of metal materials are increased.

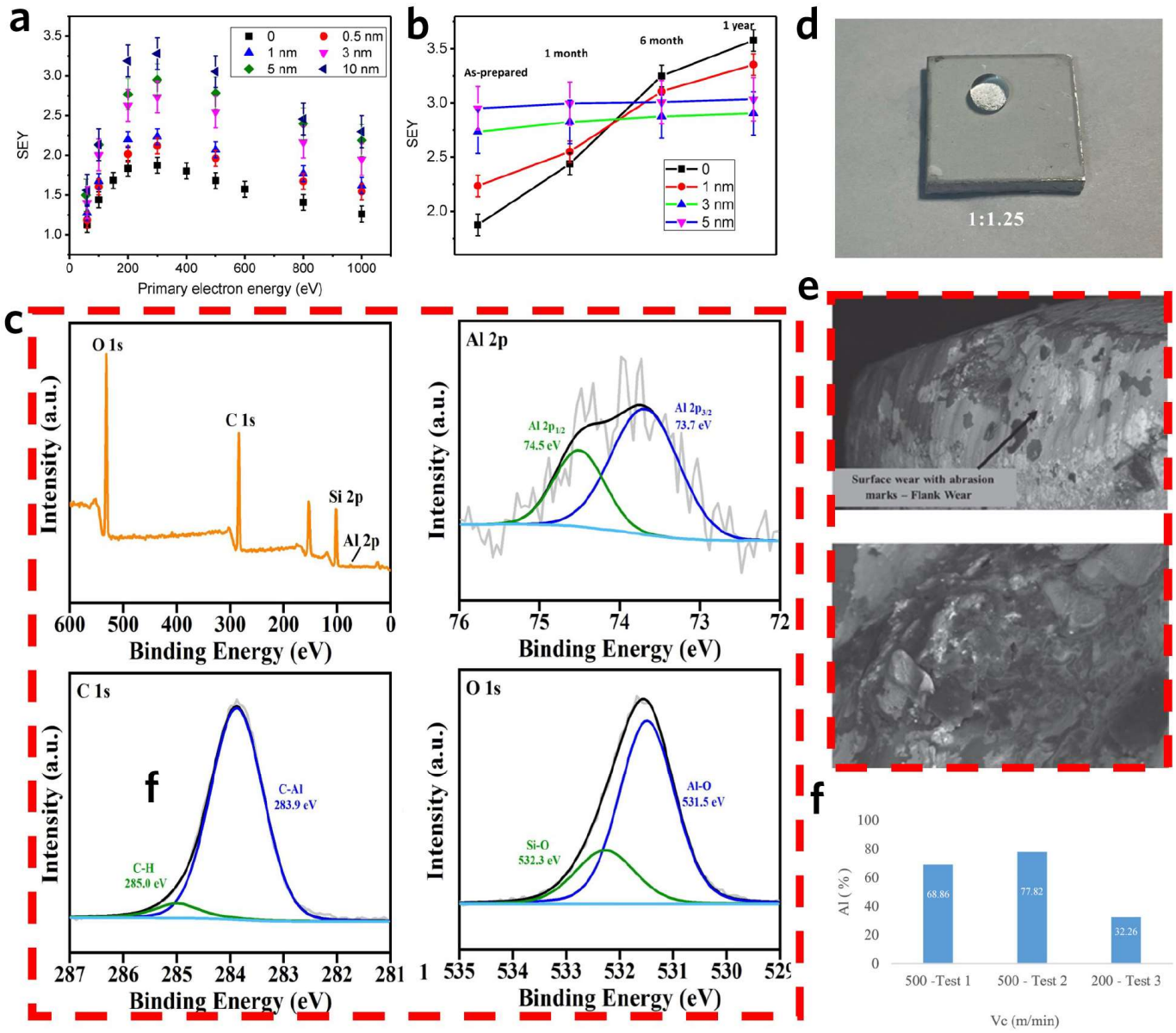

Figure 12. (**a**) The SEY as a function of primary electron energy with different thicknesses. (**b**) The change of SEY_{max} with time. (**c**) XPS full spectrum and fitted partial spectrum of the superhydrophobic coating surface. (**d**) The contact state between the droplet and the coating corresponds. (**e**) SEM on the edge of the ceramic tool with wear marks on the surface. (**f**) Correlation table with velocity cutting.

4.3.2. Industrial Furnaces and Kilns

Al_2O_3-based materials have an important practical value and a promising future in industrial furnaces and kilns. Al_2O_3-based materials are ideally suited to withstand the harsh, high-temperature environments typically encountered in industrial furnaces and kilns, particularly in industries such as steelmaking, power generation, ceramics, and glass manufacturing. Al_2O_3-based materials are commonly used in furnace bodies, walls, and linings to effectively insulate the interior of furnaces, reducing heat loss and improving overall energy efficiency. In addition, they prevent direct contact with corrosive gases, thereby reducing the risk of corrosion damage to the equipment and helping to protect the furnace structure. Al_2O_3-based refractories maintain thermal stability in furnaces, prevent premature degradation of the furnace lining, and extend the service life of the equipment. Al_2O_3-based materials are commonly used as wear-resistant linings and components in high-temperature thermal equipment, such as industrial furnaces and kilns, which must withstand significant impact, friction, and mechanical stress. Not only do these materials need to resist extreme temperatures, but they also need to exhibit sufficient wear resistance to prevent excessive wear over time. This helps minimize maintenance costs and ensures the continued efficient operation of the equipment.

5. Recent Advances and Innovations

5.1. New Formulations and Additives

In recent years, notable advancements have been made in the development of new formulations and additives for Al_2O_3-based materials, particularly in enhancing thermal conductivity, improving mechanical properties, and optimizing surface characteristics. These innovations have significantly expanded the scope and efficiency of Al_2O_3 applications, particularly in aerospace and automotive electronics.

In terms of mechanical properties, the inherent brittleness of Al_2O_3 limits its application in certain high-strength environments. However, by doping with rare earth metals and transition metal oxides, the toughness and crack resistance of Al_2O_3 have been significantly enhanced [74,75]. These modifications not only improve crack resistance but also increase the material's reliability in high-stress applications, such as those encountered in the aerospace and automotive industries.

Furthermore, the surface properties of Al_2O_3 have been optimized, particularly in terms of corrosion and oxidation resistance. Doping with elements like magnesium and calcium or employing advanced surface coating technologies has led to improvements in both corrosion resistance and thermal stability [76–78]. These enhancements extend the material's service life in harsh environments.

Innovations in new formulations and additives for Al_2O_3-based materials have significantly enhanced their performance, enabling them to excel in a wide range of advanced technological applications. As material science continues to evolve, Al_2O_3 matrix composites are poised to maintain a critical role in sectors such as high-power electronics, new energy vehicles, 5G communications, and beyond. These advancements are expected to drive further technological progress and innovation across various industries.

5.2. Development of Hybrid Materials

The latest advancements in Al_2O_3-based materials within the realm of hybrid materials are primarily reflected in innovations in composite technology and the broadening of multi-disciplinary applications. Due to its exceptional high-temperature and corrosion resistance, coupled with its high mechanical strength, Al_2O_3 has become a critical component in the development of high-performance composites across a wide range of industries.

The innovation of preparation processes plays a pivotal role in the advancement of Al_2O_3-based materials. Techniques such as the sol-gel method and solid-phase reaction have significantly improved the densification and uniformity of Al_2O_3-based composites, thereby enhancing their high-temperature stability and oxidation resistance [79]. Furthermore, the integration of 3D printing technologies has enabled Al_2O_3 matrix composites to exhibit distinct advantages in the fabrication of complex geometries and high-performance components [80]. This has facilitated the development of innovative applications in industries such as aerospace, automotive, and beyond.

In summary, Al_2O_3-based materials not only enhance the intrinsic properties of materials but also expand their application scope through advanced composite technologies and innovative manufacturing processes. As technological advancements continue to progress, Al_2O_3 matrix composites are poised to play a critical role in high-end manufacturing and cutting-edge technological fields, driving their widespread application in areas such as thermal management, electronic packaging, aerospace, and beyond.

5.3. Emerging Technologies and Future Trends

With the continuous advancements in materials science, Al_2O_3-based materials, recognized as high-performance engineering ceramics, are increasingly being integrated into emerging technologies, expanding the scope of their applications across various industries. In recent years, research on Al_2O_3-based materials has progressively shifted towards the development of higher-performance, multifunctional composites. These innovations not only enhance the fundamental properties of Al_2O_3-based materials but also unlock new application potential. Moving forward, research on Al_2O_3-based materials will focus on several cutting-edge technologies, with particular emphasis on innovations in sectors such as new energy, electronics, aerospace, and others.

In the aerospace sector, the development of Al_2O_3-based matrix composites is gaining significant momentum. When combined with carbon fiber or other ceramic matrix materials, Al_2O_3 composites exhibit enhanced strength, toughness, and high-temperature resistance, making them ideal for extreme conditions such as high-speed flight and thermal protection [81,82]. These composite materials are increasingly essential in applications like jet engines and rocket propulsion systems, where they serve as key components for thermal protection and structural integrity.

Looking ahead, advancements in Al_2O_3-based materials will focus on enhancing their overall performance and functionality. This will be achieved through techniques such as nanosizing, doping, and surface modification, which aim to further improve their mechanical, thermal, and electrical properties. As a green, environmentally friendly, and sustainable material, Al_2O_3-based materials are poised to play an increasingly vital role in the future of technology.

6. Challenges and Future Directions

6.1. Current Limitations

6.1.1. Brittleness and Mechanical Failure at High Temperatures

The extensive use of ceramic materials is predicated upon their favorable chemical and mechanical stability at elevated temperatures. However, due to the inherent brittleness of alumina ceramic materials, characterized by low fracture strength and low fracture toughness, they are susceptible to fracture and the formation of cracks in response to external forces [83]. Cracks can readily propagate in ceramic materials. Even when the impact load is below the strength threshold of the ceramic material, the material will fail during the application process. The toughening mechanism can be effectively activated by means of crack bridging, crack deflection, or phase transformation toughening, thereby enhancing the resistance of ceramic materials to crack propagation. Thus far, there are two principal methods. One such method is microstructure refinement, which serves to reduce the size of defects by reducing the size of the grains and subsequently reducing the number of defects [84]. The alternative approach is the defect tolerance method, which permits the inherent or induced defects to be accommodated through the utilization of particular techniques (such as the introduction of ductile phases). However, these two methods typically result in a compromise in the strength, stiffness, and high-temperature stability of the material. Furthermore, the mechanical properties of continuous oxidation fibers will undergo a decline during the densification process. The inherent contradiction between high toughness and mechanical properties represents a significant challenge to the application of ceramic materials. The challenge of combining high toughness with excellent mechanical properties represents a significant obstacle to the utilization of ceramic materials [85].

6.1.2. Cost and Scalability of Production

Despite decades of research on alumina-based materials, significant obstacles to their industrial implementation persist [86]. One of the most significant obstacles is the elevated cost and high energy consumption associated with the preparation of the material, which renders the scaling-up of production a challenging endeavor. The preparation of alumina materials can be broadly classified into three main categories: solid-phase synthesis, gas-phase synthesis, and liquid-phase synthesis [87]. Alumina exhibits a range of crystal structures, with transitions between phases often requiring significant energy consumption. Consequently, the production process typically necessitates high temperatures, which presents challenges in maintaining material uniformity. Furthermore, the high energy demand increases production costs. While gas phase technologies, such as chemical vapor deposition and sputtering, can also be employed to prepare alumina materials, these technologies are frequently constrained to the production of thin films on substrates. Furthermore, they necessitate the use of costly and complex vacuum equipment, which is not conducive to large-scale applications. Sol-gel method is a low-temperature synthesis method, but at present, the main precursor used is high-cost alcohol salt. On the other hand, the alcohol produced by the hydrolysis of alcohol ketones is easy to remain in the final material, which is usually harmful to the material. In addition, during the synthesis process, factors such as temperature, humidity, pH value, counterions, and concentration will affect the final performance of alumina-based materials. Therefore, how to achieve control of process parameters in large-scale production is another difficult problem faced. To summarize, the cost and large-scale application of alumina-based materials continue to encounter significant challenges, including elevated raw material costs, intricate preparation procedures, and the high energy consumption of production equipment, which constraints impede the advancement of this field.

6.1.3. Environmental Concerns and Recycling Issues

The current industrial process for the production of alumina primarily utilizes bauxite as the primary raw material, employing the Bayer process. However, this process is accompanied by a series of significant environmental risks, including the release of substantial quantities of carbon, the emission of volatile organic compounds, and the treatment of accumulated bauxite slag (commonly referred to as “red mud”). In a humid environment, bauxite slag is prone to the generation of flammable or toxic gases, including methane, hydrogen, and ammonia. Moreover, the bauxite slag

contains heavy metals, including Cd, Cr, and Pb, which have the potential to percolate into the soil and water systems, resulting in adverse effects on animal and plant life. It is of particular significance that bauxite slag contains a considerable quantity of alkaline substances, including sodium hydroxide (NaOH) and sodium silicate (Na_2SiO_3), in addition to a substantial number of valuable resources. It has been established that bauxite slag comprises approximately 30–50 wt% iron oxide and 15–25 wt% residual alumina. It is estimated that between 36 and 60 million tons of iron oxide and 18 and 30 million tons of alumina are discarded in bauxite slag annually. Consequently, the recycling and utilization of bauxite slag represent a significant challenge [88].

6.2. Research Directions

Notwithstanding the considerable advances made in the study of alumina-based materials with respect to insulation, high-temperature heat insulation, and fracture resistance, the application and production processes of alumina-based materials still encounter numerous constraints. To address these challenges, this paper outlines potential research directions, including:

(1) The contradiction between fracture resistance and excellent mechanical properties remains a significant challenge. The performance of alumina-based materials is influenced by several factors, such as particle size, morphology, composition, porosity, and crystal phase.It is therefore recommended that key basic theoretical research be conducted and the deep-level relationship between material composition, structure, process, and performance clarified. This will facilitate breakthroughs in mechanical properties, high-temperature resistance, and fracture resistance of alumina-based materials and promote the application of alumina-based materials in aerospace, electronic components, industrial furnaces, and other fields.

(2) In the future, alumina-based materials should be developed with a focus on reducing costs while avoiding methods that involve high temperatures and high pressures, reducing energy consumption in the synthesis process, and the use of expensive large-scale vacuum equipment. Furthermore, researchers should investigate the potential of low-temperature synthesis methods, such as sol-gel strategies, which are relatively simple and easily scalable. Furthermore, low-cost aluminum salts may also be employed as precursors, and the synthesis process can be optimized to guarantee the uniformity and stability of the resultant material.

(3) In the context of constrained bauxite resources, the investigation of techniques to extract alumina from low-cost and widely accessible aluminium-rich materials assumes great significance, both from the standpoint of cost reduction and the promotion of a sustainable circular economy. In addition, the development of new alumina extraction processes and methods for the reduction of emissions of harmful substances during alumina synthesis must be addressed with urgency in order to achieve low-carbon and environmentally friendly green development.

In summary, Figure 13 demonstrates the current challenges and future directions for the application of alumina-based materials in high-temperature thermal insulation, and we hoped that the advantages of alumina-based materials can be maximized, leading to better development in high-temperature thermal insulation.

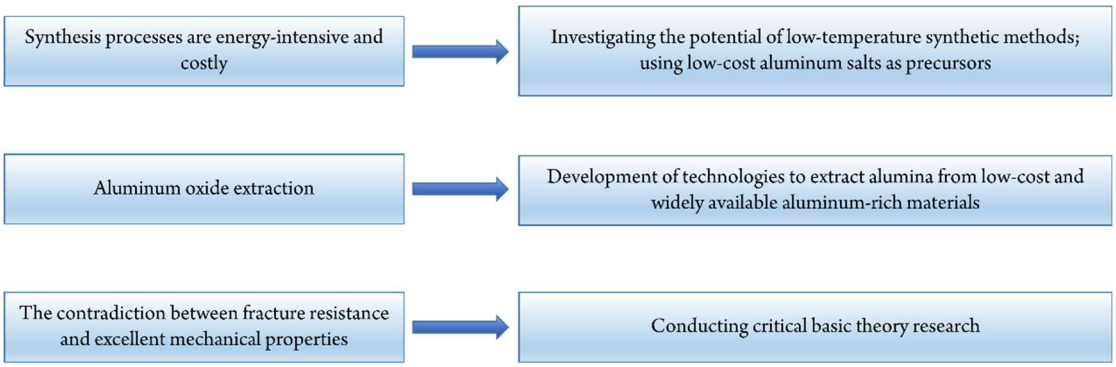

Figure 13. Challenges and future directions.

7. Conclusions and Outlook

In summary, alumina-based materials have proven to be versatile and essential in a wide range of high-performance applications, particularly in fields such as aerospace, automotive, advanced manufacturing, and industrial furnaces. Their exceptional mechanical strength, corrosion resistance, and thermal stability make them ideal for use in demanding

environments where high temperatures, thermal shock, and wear resistance are critical. The key properties that make alumina a preferred material for many industries include its high melting point, low thermal conductivity, and high compressive strength, which collectively contribute to its ability to withstand extreme conditions and enhance the longevity of components. In addition to their mechanical and thermal advantages, alumina ceramics have a wide range of applications, from wear-resistant products like grinding media and cutting tools to structural components in gas turbines and automotive parts. The use of alumina-based ceramics in high-temperature insulation is also an area of significant interest, with materials such as aerogels, powders, and coatings emerging as viable options for reducing heat transfer in industrial applications. Despite these advantages, the inherent brittleness of alumina remains a major challenge, limiting its broader adoption in certain high-stress applications. This issue underscores the ongoing need for material innovations that can improve toughness and reduce brittleness without compromising the desirable properties of alumina. Advances in the rational design of alumina compositions, microstructures, and morphologies offer promising solutions to overcome these limitations. Research efforts aimed at improving the toughness of alumina-based materials through the development of composites, hybrid materials, and novel synthesis methods are critical to expanding their scope of applications and enhancing their performance in real-world environments.

The outlook for alumina-based materials is promising, with significant potential for further development across multiple domains. Key areas of focus include enhancing the material's toughness and durability. While alumina is known for its excellent mechanical strength, its brittleness remains a limitation in high-stress environments. Future research will focus on creating alumina composites with tougher phases, such as zirconia or silicon carbide, to improve fracture toughness and impact resistance. Advanced synthesis and fabrication techniques, including additive manufacturing and high-throughput synthesis, will facilitate the development of tailored, complex structures with superior properties. Nanostructuring alumina materials offer exciting possibilities, as manipulating particle size, distribution, and morphology at the nanoscale can enhance their thermal, mechanical, and catalytic properties. Additionally, alumina's role in energy applications is set to expand, particularly in high-performance thermal insulation for energy-intensive industries like aerospace and power generation. Alumina-based aerogels are especially promising for ultra-low-density, high-performance thermal insulation. As environmental sustainability becomes increasingly important, research into recycling alumina from industrial waste streams, such as red mud, and developing eco-friendly composites will help reduce the environmental impact of alumina production. Lastly, the industrial adoption of advanced alumina-based materials will depend on cost-effective production methods and their integration into high-tech applications in automotive, aerospace, and electronics, requiring close collaboration between material scientists and industry stakeholders.

Author Contributions

Conceptualization, Y.X. and D.C.; Data Curation, Y.S., Q.Z., S.L., Z.C., Writing-Original Draft Preparation, Y.S., Q.Z., S.L., Z.C.; Writing-Review & Editing, Y.X.; Visualization, Y.S., Q.Z.; Project Administration, D.C.; Funding Acquisition, X. J., D.C.

Ethics Statement

Not applicable.

Informed Consent Statement

Not applicable.

Funding

This work was financially supported by the Young Scholars Program of Shandong University, the National Natural Science Foundation of China (grant 22275116), and the Natural Science Foundation of Shandong Province (Major Basic Research) project (grant ZR2023ZD19).

Declaration of Competing Interest

The authors declare no competing financial interest.

References

1. Meetham GW. High-temperature materials—A general review. *J. Mater. Sci.* **1991**, *26*, 853–860.
2. Krasnovskih MP, Maksimovich NG, Vaisman YI, Ketov AA. Thermal stability of mineral-wool heat-insulating materials. *Russ. J. Appl. Chem.* **2014**, *87*, 1430–1434.
3. Wang H, Zhang X, Wang N, Li Y, Feng X, Huang Y, et al. Ultralight, scalable, and high-temperature–resilient ceramic nanofiber sponges. *Sci. Adv.* **2017**, *3*, e1603170.
4. Xu X, Zhang Q, Hao M, Hu Y, Lin Z, Peng L, et al. Double-negative-index ceramic aerogels for thermal superinsulation. *Science* **2019**, *363*, 723–727.
5. An L, Armstrong JN, Hu Y, Huang Y, Li Z, Zhao D, et al. High temperature ceramic thermal insulation material. *Nano Res.* **2022**, *15*, 6662–6669.
6. Ji Q, Chen Z, Xing S, Jiao X, Chen D. Mullite Nanosheet/Titania Nanorod/Silica Composite Aerogels for High-Temperature Thermal Insulation. *ACS Appl. Nano Mater.* **2023**, *6*, 17218–17228.
7. Xu B, Yang Y, Xu Y, Han B, Wang Y, Liu X, et al. Synthesis and characterization of mesoporous Si-modified alumina with high thermal stability. *Microporous Mesoporous Mater.* **2017**, *238*, 84–89.
8. Chen G, Wang Y, Zou Y, Wang H, Qiu J, Cao J, et al. Hexagonal boron nitride and alumina dual-layer coating for space solar thermal shielding. *Chem. Eng. J.* **2021**, *421*, 127802–127808.
9. Zhang B, Zhang X, Wang C, Zhang Y, Yang J. Facile method for preparing lamellar structured alumina-zirconia ceramics with high toughness. *Ceram. Int.* **2023**, *49*, 3070–3075.
10. Han X-X, Zhang T-A, Lv G-Z, Pan X-J, Fu D-X. Effects of Additives on Alumina Preparation from Aluminum Chloride Solution by Electrolytic Transformation. *JOM* **2019**, *71*, 1574–1580.
11. Zhu J, Li J, Zhang H. CFD Investigation of Bath Flow and Its Related Alumina Transmission in Aluminum Reduction Cells: Slotted Anodes and Busbar Designs. *Metals* **2020**, *10*, 805.
12. Nnanwube IA, Keke M, Onukwuli OD. Kinetics of Owhe kaolinite leaching for alumina recovery in hydrochloric acid solution. *Sci. Afr.* **2024**, *23*, e02045–e02056.
13. Chen R, Shi L, Huang H, Yuan J. Extraction of Iron and Alumina from Red Mud with a Non-Harmful Magnetization Sintering Process. *Minerals* **2023**, *13*, 452.
14. Zhao Q, Zhao M, Jiao X, Xia Y, Chen D. Unraveling the Structural Evolution of Aluminum Polyoxocations in Solution. *Langmuir* **2024**, *40*, 20284–20293.
15. González-Solórzano MG, Morales R, Ávila JR, Muñiz-Valdés CR, Bastida AN. Alumina Nucleation, Growth Kinetics, and Morphology: A Review. *Steel Res. Int.* **2023**, *94*, 2200678–2200709.
16. Chandran CV, Kirschhock CEA, Radhakrishnan S, Taulelle F, Martens JA, Breynaert E. Alumina: discriminative analysis using 3D correlation of solid-state NMR parameters. *Chem. Soc. Rev.* **2019**, *48*, 134–156.
17. Buwono HP, Adiwidodo S, Wicaksono H, Firmansyah HI. Hydrothermal synthesis and characterization of nano-particles γ-Al_2O_3. *IOP Conf.Ser. Mater. Sci. Eng.* **2021**, *1073*, 012011–012016.
18. Wang Z, Wei Y-M, Xu Z-L, Cao Y, Dong Z-Q, Shi X-L. Preparation, characterization and solvent resistance of γ-Al_2O_3/α-Al_2O_3 inorganic hollow fiber nanofiltration membrane. *J. Membr. Sci.* **2016**, *503*, 69–80.
19. Aksel C. The role of fine alumina and mullite particles on the thermomechanical behaviour of alumina–mullite refractory materials. *Mater. Lett.* **2002**, *57*, 708–714.
20. Shi R, Shang Y, Zhang Y, Wang P, Zhang A, Yang P. Synthesis of ultrafine α-Al_2O_3 powder by two-step hydrolysis. *Ceram. Int.* **2018**, *44*, 3741–3750.
21. Vera-Londono L, Ruiz-Clavijo A, Caballero-Calero O, Martín-González M. Understanding the thermal conductivity variations in nanoporous anodic aluminum oxide. *Nanoscale Adv.* **2020**, *2*, 4591–4603.
22. Bodapati A, Keblinski P, Schelling PK, Phillpot SR. Crossover in thermal transport mechanism in nanocrystalline silicon. *Appl. Phys. Lett.* **2006**, *88*, 141908.
23. Ghica ME, Almeida CMR, Rebelo LSD, Cathoud-Pinheiro GC, Costa BFO, Durães L. Novel Kevlar® pulp-reinforced alumina-silica aerogel composites for thermal insulation at high temperature. *J. Sol-Gel Sci. Technol.* **2022**, *101*, 87–102.
24. Liu S, Shah M, Rao S, An L, Mohammadi MM, Kumar A, et al. Flame aerosol synthesis of hollow alumina nanoshells for application in thermal insulation. *Chem. Eng. J.* **2022**, *428*, 131273.
25. Zemtsova EG, Monin AV, Smirnov VM, Semenov BN, Morozov NF. Formation and mechanical properties of alumina ceramics based on Al_2O_3 micro- and nanoparticles. *Phys. Mesomech.* **2015**, *18*, 134–138.
26. Shuai Y, Ai J, Hu L, Xu H, Cheng L, Chen Z, et al. Residual strength of porous alumina ceramics and fractal characterization of their crack patterns after thermal shocks. *Ceram. Int.* **2024**, *50*, 41848–41856.
27. Castillo-Rodríguez M, Muñoz A, Domínguez-Rodríguez A. Creep study on alumina and alumina/SWCNT nanocomposites. *J. Eur. Ceram. Soc.* **2018**, *38*, 5497–5502.
28. Zhang J, Liu F, Liu P, He D. Transparent Alumina Nanoceramics Prepared under High Pressure and Low Temperature. *Adv. Eng. Mater.* **2023**, *25*, 2101413–2101418.

29. Yang R, Qi Z, Gao Y, Yang J, Zhou Y, Liu H, et al. Effects of alumina sols on the sintering of α-alumina ceramics. *Ceram. Int.* **2020**, *46*, 20865–20870.
30. Awang Chee DN, Ismail AF, Aziz F, Amin MAM, Abdullah N. The influence of alumina particle size on the properties and performance of alumina hollow fiber as support membrane for protein separation. *Sep. Purif. Technol.* **2020**, *250*, 117147.
31. Cox BN, Zok FW. Advances in ceramic composites reinforced by continuous fibers. *Curr. Opin. Solid State Mater. Sci.* **1996**, *1*, 666–673.
32. Wang X, Tian Y, Yu C, Liu L, Zhang Z, Wu Y, et al. Organic/inorganic double-precursor cross-linked alumina aerogel with high specific surface area and high-temperature resistance. *Ceram. Int.* **2022**, *48*, 17261–17269.
33. Hadian A, Duckek J, Parrilli A, Liersch A, Clemens F. Additive Manufacturing of Fiber-Reinforced Zirconia-Toughened Alumina Ceramic Matrix Composites by Material Extrusion-Based Technology. *Adv. Eng. Mater.* **2024**, *26*, 2302158.
34. Gopalan H, Chokshi AH. Creep in alumina and carbon nanotube reinforced alumina composites. *Mater. Sci. Eng. A* **2018**, *731*, 561–568.
35. Hashimoto RY, Menon ESK, Fox AG. Segregation of Silicon in Metal-Alumina Composites. *Microsc. Microanal.* **1999**, *5* (S2), 624–625.
36. Kokatev AN, Lukiyanchuk IV, Yakovleva NM, Rudnev VS, Chupakhina EA, Yakovlev AN, et al. Catalytically active composite materials with porous aluminum oxide matrix modified by γ-MnO_2 nanoparticles. *Prot. Met. Phys. Chem. Surf.* **2016**, *52*, 832–838.
37. Zhang XL, Liang MK, Sun FH, Xu DF. Thermal insulating performance of thermal protection system with sandwich structure based on Al_2O_3/SiC composites aerogels. *Ceram. Int.* **2024**, *50*, 33946–33952.
38. Peng F, Jiang YG, Feng J, Cai HF, Feng JZ, Li LJ. Thermally insulating, fiber-reinforced alumina–silica aerogel composites with ultra-low shrinkage up to 1500 °C. *Chem. Eng. J.* **2021**, *411*, 128402.
39. Zu GQ, Shen J, Wang WQ, Zou LP, Lian Y, Zhang ZH, et al. Robust, Highly Thermally Stable, Core–Shell Nanostructured Metal Oxide Aerogels as High-Temperature Thermal Superinsulators, Adsorbents, and Catalysts. *Chem. Mater.* **2014**, *26*, 5761–5772.
40. Huang RM, Jiang YG, Feng JZ, Li LJ, Hu YJ, Wang XQ, et al. Robust and exceptional thermal insulating alumina-silica aerogel composites reinforced by ultra IR-opacified ZrO_2 nanofibers. *Chem. Eng. J.* **2024**, *498*, 155283.
41. Ji QY, Zhang L, Jiao XL, Chen DR. Alpha Al_2O_3 Nanosheet-Based Biphasic Aerogels with High-Temperature Resistance up to 1600 °C. *ACS Appl. Mater. Interfaces* **2023**, *15*, 6848–6858.
42. Jiang JP, Yan LW, Li JT, Xue YJ, Zhang CS, Hu XX, et al. Lightweight, thermally insulating SiBCN/Al_2O_3 ceramic aerogel with enhanced high-temperature resistance and electromagnetic wave absorption performance. *Chem. Eng. J.* **2024**, *501*, 157656.
43. Luo JH, Yang DY, Wei LW, Li X, Zhao JJ, Hao MX, et al. Thermal insulation characteristics of roll forming alumina ball material. *Ceram. Int.* **2021**, *47*, 16491–16499.
44. Liu JF, Li YB, Li SJ, Chen P. Novel nanometer alumina-silica insulation board with ultra-low thermal conductivity. *Ceram. Int.* **2022**, *48*, 10480–10485.
45. Sun LJ, Dong P, Zeng Y, Chen JM. Fabrication of hollow lattice alumina ceramic with good mechanical properties by Digital Light Processing 3D printing technology. *Ceram. Int.* **2021**, *47*, 26519–26527.
46. Wang LK, Feng JZ, Luo Y, Jiang YG, Zhang GJ, Feng J. Versatile Thermal-Solidifying Direct-Write Assembly towards Heat-Resistant 3D-Printed Ceramic Aerogels for Thermal Insulation. *Small Methods* **2022**, *6*, 2200045.
47. Yang GY, Guan RH, Zhen HY, Ou KT, Fang J, Li DS, et al. Tunable Size of Hierarchically Porous Alumina Ceramics Based on DIW 3D Printing Supramolecular Gel. *ACS Appl. Mater. Interfaces* **2022**, *14*, 10998–11005.
48. Alhendi M, Alshatnawi F, Alshatnawi F, Sivasubramony R, Khinda G, Umar AI, et al. Printed electronics for extreme high temperature environments. *Addit. Manuf.* **2022**, *54*, 102709.
49. Alshatnawi F, Enakerakpo E, Alhendi M, Abdelatty M, Umar A, Al-Haidari R, et al. High stability and reliability additively manufactured metal-insulator-metal capacitors for high-temperature applications. *Mater. Today Commun.* **2024**, *39*, 108682.
50. Obeidat AS, Umar A, Dou Z, Alshatnawi F, Al-Haidari R, Al-Shaibani W, et al. Embedded RF Packaging Via Ceramic 3D Printing and Printed Electronics Additive Manufacturing. In Proceedings of the 2024 IEEE 74th Electronic Components and Technology Conference (ECTC), Denver, CO, USA, 28–31 May 2024; pp. 685–692.
51. Xia B, Wang ZP, Gou LZ, Zhang M, Guo M. Porous mullite ceramics with enhanced compressive strength from fly ash-based ceramic microspheres: Facile synthesis, structure, and performance. *Ceram. Int.* **2022**, *48*, 10472–10479.
52. Wang N, Xie YS, Lv JA, Zhang J, Zhu LY, Jia ZT, et al. Preparation of ultrafine flexible alumina fiber for heat insulation by the electrospinning method. *Ceram. Int.* **2022**, *48*, 19460–19466.
53. Guan C, Xu Z, Zhu H, Lv X, Liu Q. Insights into the mechanism of fluoride adsorption over different crystal phase alumina surfaces. *J. Hazard. Mater.* **2022**, *423*, 127109.
54. Ma Y, Peng S, Liu W, Yao S, Wang J. Preparation of a dense alumina fiber with nanograins by a novel two-step calcination. *J. Sol-Gel Sci. Technol.* **2022**, *103*, 125–138.
55. Patel K, Blair V, Douglas J, Dai Q, Liu Y, Ren S, et al. Structural Effects of Lanthanide Dopants on Alumina. *Sci. Rep.* **2017**,

7, 39946.
56. Lamouri S, Hamidouche M, Bouaouadja N, Belhouchet H, Garnier V, Fantozzi G, et al. Control of the γ-alumina to α-alumina phase transformation for an optimized alumina densification. *Boletín de la Sociedad Española de Cerámica y Vidrio* **2017**, *56*, 47.
57. Liu LG, Yu H, Wang JZ, Wang LJ, Jiang W, Li JL. In situ carbon nanonetwork structure based on MOF-derived carbon to manufacture ceramic composites: A case study of zirconia-toughened alumina. *Ceram. Int.* **2024**, *50*, 42135–42145.
58. Wu CZ, Liu Q, Chen R, Wang J, Liu WS, Yao SW, et al. Mechanism of grain refinement and growth for the continuous alumina fibers by MgO addition. *Ceram. Int.* **2023**, *49*, 8565–8575.
59. Jiang R, Yang LW, Liu HT, Sun X, Cheng HF. High-temperature mechanical properties of Nextel^{TM} 610 fiber reinforced silica matrix composites. *Ceram. Int.* **2018**, *44*, 15356–15361.
60. Dong X, An QL, Zhang SP, Yu HY, Wang MC. Porous ceramics based on high-thermal-stability Al_2O_3–ZrO_2 nanofibers for thermal insulation and sound absorption applications. *Ceram. Int.* **2023**, *49*, 31035–31045.
61. Bie C, Sang S, Li Y, Zhu T, Xu Y. Research of Al_2O_3-SiC-C refractories as chromia-free lining for gasifier. *Ceram. Int.* **2016**, *42*, 14161–14167.
62. Jiao YM, Song Q, Yang X, Han LY, Xiao CX, Zhao F, et al. Mechanical and electromagnetic interference shielding properties of *in-situ* grown Si_3N_4nw synergistic defective-graphene reinforced alumina ceramics. *Compos. Part B Eng.* **2025**, *289*, 111945.
63. He DL, Ou DB, Gao H, Jiao FK. Thermal insulation and anti-vibration properties of $MoSi_2$-based coating on mullite fiber insulation tiles. *Ceram. Int.* **2022**, *48*, 1844–1850.
64. Shimizu T, Matsuura K, Furue H, Matsuzak K. Thermal conductivity of high porosity alumina refractory bricks made by a slurry gelation and foaming method. *J. Eur. Ceram. Soc.* **2013**, *33*, 3429–3435.
65. Hossain SS, Baek I-W, Son H-J, Park S, Bae C-J. 3D printing of porous low-temperature *in-situ* mullite ceramic using waste rice husk ash-derived silica. *J. Eur. Ceram. Soc.* **2022**, *42*, 2408–2419.
66. Cao YQ, Xu XJ, Qin Z, He C, Yan LW, Hou F, et al. Vat photopolymerization 3D printing of thermal insulating mullite fiber-based porous ceramics. *Addit. Manuf.* **2022**, *60*, 103235.
67. Xie GB, Bai HW, Miao GH, Feng GB, Yang J, He Y, et al. The Applications of Ultra-Thin Nanofilm for Aerospace Advanced Manufacturing Technology. *Nanomaterials* **2021**, *11*, 3282.
68. Li B, Li X. Efficient and Controllable Preparation of Super-Hydrophobic Alumina-Based Ceramics Coating on Aviation Al-Li Alloy Surface for Corrosion Resistance and Anti-Icing Behavior. *Coatings* **2024**, *14*, 1223.
69. Sousa TA, De Paula MA, Konatu RT, Ribeiro MV, De Campos E, Souza JVC. Investigation of the performance of ceramic tools of alumina doped with magnesium oxide in the dry machining of compacted graphite iron. *Mater. Res. Express* **2019**, *6*, 046546.
70. Hussainova I, Baronins J, Drozdova M, Antonov M. Wear performance of hierarchically structured alumina reinforced by hybrid graphene encapsulated alumina nanofibers. *Wear* **2016**, *368–369*, 287–295.
71. Chauhan V, Bijwe J, Darpe A. Functionalization of alumina particles to improve the performance of eco-friendly brake-pads. *Friction* **2021**, *9*, 1213.
72. Shen MX, Li B, Zhang ZN, Zhao LZ, Xiong GY. Abrasive wear behavior of PTFE for seal applications under abrasive-atmosphere sliding condition. *Friction* **2019**, *8*, 755.
73. Drdlikova K, Drdlik D, Hadraba H, Klement R, Maca K. Optical and mechanical properties of mn-doped transparent alumina and their comparison with selected rare earth and transient metal doped aluminas. *J. Eur. Ceram. Soc.* **2020**, *40*, 4894.
74. Han BH, Key B, Lapidus SH, Garcia JC, Iddir H, Vaughey JT, et al. From Coating to Dopant: How the Transition Metal Composition Affects Alumina Coatings on Ni-Rich Cathodes. *ACS Appl. Mater. Interfaces* **2017**, *9*, 41291–41302.
75. Salman M, Bae H-M, Yoon D-H. Joining of alumina using magnesium- or calcium-aluminosilicate glass–ceramic fillers. *Ceram. Int.* **2022**, *48*, 21532–21542.
76. Zhang XL, Gu JH, Ye Q, Zhang YQ, Zhang Q, Cheng CX, et al. Thermal energy storage performance of magnesium-based hydrated salts impregnated with activated alumina. *Energy Sources Part A RecoveryUtil. Environ. Eff.* **2023**, *45*, 10487–10504.
77. Zhang F, Zuo Y, Wu D, Yang G, Schubert DW, Nie L. Hydrophobic Alumina Coatings for Magnesium Substrates with Advancing Electromagnetic Wave Absorption Capability. *J. Mater. Eng. Perform.* **2024**, *31*, 1–8.
78. ElDeeb AB, Brichkin VN, Bertau M, Savinova YA, Kurtenkov RV. Solid state and phase transformation mechanism of kaolin sintered with limestone for alumina extraction. *Appl. Clay Sci.* **2020**, *196*, 105771.
79. DeVries M, Subhash G, McGhee A, Ifju P, Jones T, Zheng J, et al. Quasi-static and dynamic response of 3D-printed alumina. *J. Eur. Ceram. Soc.* **2018**, *38*, 3305.
80. Bach M, Gehre P, Biermann H, Aneziris CG. Recycling of carbon fiber composites in carbon-bonded alumina refractories. *Ceram. Int.* **2020**, *46*, 12574–12583.
81. Fan CY, Ma QS, Zeng KH. Microstructure and mechanical properties of carbon fibre-reinforced alumina composites fabricated from sol. *Bull. Mater. Sci.* **2018**, *41*, 68.
82. Qi F, Meng S, Song F, Guo H, Xu X, Shao Y, et al. Fractal characterization of ceramic crack patterns after thermal shocks. *J.*

Am. Ceram. Soc. **2019**, *102*, 3641.
83. Ighodaro OL, Okoli OI. Fracture Toughness Enhancement for Alumina Systems: A Review. *Int. J. Appl. Ceram. Technol.* **2008**, *5*, 313.
84. Smith P, Power G. High Purity Alumina—Current and Future Production. *Miner. Process. Extr. Metall. Rev.* **2022**, *43*, 747.
85. Lee D-H, Han S-S, Kim Y-H, Lim S-K. Analysis of crystal phases of Na+-*β/β*”-alumina/YSZ composite prepared by vapor-phase synthesis from YSZ-toughened α-alumina. *J. Ind. Eng. Chem.* **2019**, *76*, 366.
86. Niero DF, Montedo ORK, Bernardin AM. Synthesis and characterization of nano α-alumina by an inorganic sol–gel method. *Mater. Sci. Eng. B* **2022**, *280*, 115690.
87. Ma Y, Preveniou A, Kladis A, Pettersen JB. Circular economy and life cycle assessment of alumina production: Simulation-based comparison of Pedersen and Bayer processes. *J. Clean. Prod.* **2022**, *366*, 132807.
88. Zhu X, Jin Q, Ye Z. Life cycle environmental and economic assessment of alumina recovery from secondary aluminum dross in China. *J. Clean. Prod.* **2020**, *277*, 123291.